Applied Mathematical Modelling 89 (2021) 1206–1234

Contents lists available at ScienceDirect

Applied Mathematical Modelling

journal homepage: www.elsevier.com/locate/apm

Integrated modelling of sea-state forecasts for safe navigation and operational management in ports: Application in the Mediterranean Sea ☆

Christos Makris [a,*], Yannis Androulidakis [a,c], Theofanis Karambas [a,d], Andreas Papadimitriou [b,d], Anastasios Metallinos [b,d], Yiannis Kontos [a], Vassilis Baltikas [a], Michalis Chondros [b,d], Yannis Krestenitis [a], Vicky Tsoukala [b], Constantine Memos [b,d]

[a] *Laboratory of Maritime Engineering, School of Civil Engineering, Aristotle University of Thessaloniki, 54124 Thessaloniki, Greece*
[b] *Laboratory of Harbour Works, School of Civil Engineering, National Technical University of Athens, Athens, Greece*
[c] *Department of Ocean Sciences, University of Miami/Rosenstiel School of Marine and Atmospheric Science (RSMAS), Miami, FL 33149, USA.*
[d] *Scientia Maris, 15772, Agias Elenis Str. 10, Zografos, Greece*

ARTICLE INFO

Article history:
Received 17 October 2019
Revised 15 June 2020
Accepted 3 August 2020
Available online 12 August 2020

Keywords:
Integrated modelling
Surface waves
Sea level elevation
Sea state forecast
Ports
Navigation safety

ABSTRACT

In this paper we present recent evolvements of three robust numerical models for the simulation of the evolution of wave fields and hydrodynamic circulation in gulfs and coastal areas with large harbours and significant urban port facilities. The models are integrated into a single software suite for the development of a decision support tool to provide reliable forecasts of sea states prevailing at selected important ports worldwide. The application of the integrated modelling platform is designed to support approaching procedures of vessels to ports and it is based on co-operating, high-resolution, hydrodynamic (ocean and wave) models that derive input data and boundary conditions from global scale or regional, open sea and weather forecasts. The implementation of short-term forecasts for sea conditions includes the development, validation, coupling, and operational application of:

Abbreviations: 2-DH, Two-Dimensional Horizontal; AUTh, Aristotle University of Thessaloniki; AVANTI, Access to Validated Nautical Information; CMEMS, Copernicus Marine Environmental Monitoring Service; CNPs, Certified Navigation Pathways; COSYNA, Coastal Observing System for Northern and Arctic Seas; E, Percent Error; ECMWF, European Centre for Medium-Range Weather Forecasts; EI, Error Index; ESA, European Space Agency; FDM, Finite Difference Method; GEBCO, General Bathymetric Chart of the Oceans; GLOSS, Global Sea-Level Observing System; GMT, Greenwich Mean Time; HiReSS, High Resolution Storm Surge model; HNHS, Hellenic Navy Hydrographic Service; HRP, Hit Rate of Percentiles; IMO, International Maritime Organization; ISPRA, Italian National Institute for Environmental Protection and Research; MoC, Method of Characteristics; MSL, Mean Sea Level; NOAA, National Oceanic and Atmospheric Administration; RMSE, Root-Mean-Square Error; SBE26, Sea-Bird Electronics Seagauge Wave & Tide Recorder model 26; SLP, Sea Level Pressure; SOCIB, Balearic Islands Coastal Ocean Observing and Forecasting System; SSH, Sea Surface Height; SSI, Storm Surge Index; SWAN, Simulating WAves Nearshore; TOMAWAC, TELEMAC-based Operational Model Addressing Wave Action Computation; UST, Universal Standard Time; WAM, WAve Modelling cycle 4 model; WAVE-L, AUTh's hyperbolic mild-slope equation wave model; WRF-ARW, Weather Research and Forecasting model with the Advanced Research dynamic solver; WS, Willmott Skill score.

☆ This article belongs to the Special Issue: DMPCO 2019.

* Corresponding author.
E-mail addresses: cmakris@civil.auth.gr (C. Makris), iandroul@civil.auth.gr, iandroul@rsmas.miami.edu (Y. Androulidakis), karambas@civil.auth.gr (T. Karambas), andreas_papad@yahoo.com (A. Papadimitriou), anast.metallinos@gmail.com (A. Metallinos), ykontos@civil.auth.gr (Y. Kontos), vmpaltik@civil.auth.gr (V. Baltikas), mxondros@msn.com (M. Chondros), ynkrest@civil.auth.gr (Y. Krestenitis), tsoukala@mail.ntua.gr (V. Tsoukala), memos-ports@civil.ntua.gr (C. Memos).

https://doi.org/10.1016/j.apm.2020.08.015

i) the High Resolution Storm Surge (HiReSS) model for sea level variations; ii) the 3rd generation spectral wave model called TELEMAC-based Operational Model Addressing Wave Action Computation (TOMAWAC) for irregular wave propagation in offshore and coastal areas; and iii) a high resolution phase-resolving wave model (WAVE-L) for port basins, based on the hyperbolic mild-slope equations. This innovative product, designed for port-related end-users, will improve the navigation safety at ports, optimize the berth occupancy, support the port pilotage operations, mooring and towage procedures, and may facilitate the port layout upgrade or design. Hereby, pilot forecast implementations are presented concerning the Mediterranean Sea and eight selected harbours in it.

1. Introduction

1.1. Background and incentive

Intercontinental ocean and short sea shipping are important levers for both freight transport and passenger travel movement, significantly contributing to the economic and social development on a global scale, *e.g.* accounting for almost 90% of world trade. Ports are vital links in the chain of maritime transportations and have a decisive impact on their quality. The basic port operations with regard to visiting vessels include successive discrete procedures such as vessel approach by selection of Certified Navigation Pathways (CNPs), towage, selection of mooring location or berth position, freighting, arrival and departure of passengers, and sailing from and to ports. The increase in ship/vessel size and the related transport load exercise strong pressure on port authorities, which often hardly adapt to the aforementioned developments on time. This leads to an increase in both number and cost of maritime accidents, the majority of which involve collisions with other vessels, ship grounding on the port seabed or on harbour structures. The quality and safety of maritime transportations are therefore dependent on prevailing ocean and meteorological conditions in relation to the port's configuration at the time of approach.

Recent navigation safety reports show that 60% of marine accidents are human-induced [1]; the majority of vessel approach accidents could probably be avoided by means of proper navigation support tools [2]. Recent reports from the British Department for Transport [3], based on 920.000 movements of vessels in and out of 13 United Kingdom (UK) ports over the 2005–2009 period, showed that one accident occurred per 1000 movements on average, while for commercial vessels the frequency was higher, *i.e.* one accident per 240 movements. Most of the accidents occurred in the vicinity of mooring sites or exact at berth positions (45%) and along CNPs inside the port basins (40%). Almost one third (34%) of the port accidents were due to incompetent navigation. Moreover, the certification of navigation paths in port areas by the European Space Agency (ESA) conforming to the International Maritime Organization's (IMO) e-Navigation strategy requires knowledge of currently prevailing conditions including sea state and related environmental data.

We seek to investigate the impact of sea states, in terms of detailed maritime conditions' forecasting, on the abovementioned processes and the development of an operational forecast platform with a decision support tool for both port pilots and ship masters in several ports of the Mediterranean Sea. This application is developed in the framework of the research project Accu-Waves [4,5] which will cover the implementation of operational marine forecast systems to support navigation in major ports worldwide.

The background literature and relevant modelling applications generally covering met-ocean forecasts is vast, yet the existing research work focusing on the development of sea-state forecasts in port areas, based on coupling between state-of-the-art regional ocean simulations to significantly high-resolution wave simulations inside the ports, is not replete. The 24/7 delivery of near-future marine predictions to vessel operatives during their approach to ports through the user-friendly operational platform maintained by MarineTraffic [6] is an innovative product that will significantly increase navigation safety.

1.2. Literature review on previous research

The subsistent literature on operational sea-state forecasting in coastal areas concerns the short-term predictions of primarily spectral wave characteristics and secondarily ocean circulation. However, the usual spatial resolution of the implemented models is rather coarse for the detail needed in the vicinity of harbour structures and inside port facilities. This has to do mostly with the choice of phase-averaged, instead of phase-resolving, wave models and available processing resources under time-efficient computations. Selected relevant research endeavours are concisely presented below.

The Naval Research Laboratory created a wave hindcasting/forecasting system in support of the Nearshore Canyon Experiment field program with the use of Simulating WAves Nearshore (SWAN) model focusing on the coastal area in the Southern California Bight [7]. The stationary assumption for 3rd generation spectral wave model computations used in this system is criticized and crude bathymetric resolution issues are highlighted especially in areas near islands in the Bight, having strong impact on the nearshore wave climate [7]. Solutions are examined in terms of computational efficiency and

expensiveness for operational use. The proposed system [7] provides poor predictions of the swell occurrence timing and local sea growth/decay in terms of ocean boundary conditions that influence the directional distribution of wave energy in coastal areas. Besides the latter, it is also shown that resolution and accuracy issues of available local atmospheric forcing may drive erroneous results of spectral wave model predictions.

A real-time nearshore wave, tide and current prediction system was demonstrated during the Maritime Rapid Environmental Assessment 2004 Trial in Portuguese coastal waters for regional scale daily forecasts [8]. Global scale forcing input from meteorological and oceanographic centers were utilized. The attempt also focused on a limited beach experiment with Delft3D model to build a coastal hydrodynamic modelling system, in order to predict nearshore wave-induced and longshore currents near Pinheiro da Cruz. Once again, the coarseness of modelled wave forecasts had an ill influence on nearshore current reproduction [8].

An evaluation of a high-resolution operational wave forecasting system in the Adriatic Sea was performed with the use of SWAN model using wind inputs generated by ALADIN-8 operational atmospheric model [9]. Real-time surface waves' forecast was pursued in order to trace high seas and extreme waves during Bora and Sirocco wind storms. The model prediction skill was rather high, evaluated against *in situ* field measurements and altimeter observations, but referred to open sea areas compared to the analysis of nearshore data given by us in the present paper. Comparisons at five coastal stations showed that the forecast wave heights were underpredicted by an average of 30% reaching up to 50% errors. Higher-resolution wind forcing combined with realistic inland orography could decrease the observed wave forecast bias.

To ensure marine operations' safety and support, an ocean weather prediction system by three-way coupled wave forecasts was developed in Prince William Sound of USA [10]. The authors commented on the issue of wave forecast reliability that leads to uncertainty of planning, managing and engineering operations. High-resolution, 36-hours daily forecasts of significant wave heights showed an acceptable correlation with field data, but rather for open sea than nearshore areas.

Large-scale wave forecasts are operated by the European Centre for Medium-Range Weather Forecasts (ECMWF) [11]. Changes to input and dissipation source terms of WAM (WAve Modelling) Cycle 4 model were proposed in order to improve simulated wave data. Comparisons mainly referred to ocean buoys and offshore altimeter wave data, albeit for limited areas in the forecast domain not reaching the coastal fronts and port areas.

A novel paradigm in operational wave forecasting systems was presented in [12] for the National Center for Environmental Prediction using WAVEWATCH-III numerical model. The system used a mosaic of two-way nested grids in a single model implementation in order to provide suitable resolution for multiple areas of gridded forecast products. Although a spectral partitioning algorithm was introduced to separate individual sea states from the overall spectrum, thus providing additional products for multiple sea states, the system is applied on rather large-scale regions and coarse spatial resolutions.

The evaluation of a high-resolution wave forecasting system in port approaches was presented in [13]. The objective was to test the SWAN model for real-time information about sea states around Portuguese ports. Inclusion of white-capping offshore wave breaking and increase of spatial resolution led to considerable enhancement of wave prediction accuracy in nearshore areas, especially where fine bathymetry and wind data were available.

In all the aforementioned research efforts, much larger areas were investigated compared to our case presented herein. The last in dynamic downscaling succession and finest grid resolution for 3rd generation wave modelling in the aforementioned would be the starting level of our model implementations, *i.e.* the coarsest resolution in our coastal wave model coupling effort. Moreover, we hereby attempt to further use phase-resolving models in super fine resolution ($\Delta x \leq 2$ m) around ports and inside harbour basins. Finally, the coupled wave models are fed with reliable model forecasts for sea level elevation and depth-averaged currents in coastal areas due to both atmospheric forcing and astronomical tides in the context of a built-in simulation approach for tidally influenced storm surges.

1.3. Review of sea-state forecast applications

The significance of the presented research and other existing sea-state forecast platforms and applications is demonstrated by IMO's strategy under code e-Navigation [14]. The latter aims, through digital analysis and data dissemination, to reduce the adverse effects of unpredictable human factor on navigation, and thus increase competitiveness and safety of maritime transport [15]. One of the electronic services sections required in Strategic Plan 2015–2019 refer to Local Port Services including high-resolution meteorological and hydrographic data and information on mooring positions [16]. For example, the Docking Assist system [17] is an effort to support ship sailing operations in ports, according to vessel position with regard to harbour structures surrounding it at any time and therefore contributes to improving port management efficiency. A similar tool called Physical Oceanographic Real-Time System (PORTS®), developed by the USA's National Oceanic and Atmospheric Administration (NOAA), uses real-time data from US ports and provides forecasts of sea state parameters for safe inland navigation [18]. A more general application, named Access to Validated Nautical Information (AVANTI), was recently developed with initiative of the International Harbour Masters' Association and the UK Hydrographic Office and provides series of marine port information to its users online [19].

Other online modelling applications, services and platforms of mid-resolution met-ocean forecasts related to coastal areas, comprising but not necessarily focusing on ports, can be indicatively divided to the following, among many in the field:

- On a global scale, there are fully versatile, freely provided, and widely used initiatives of open data for ocean parameters, such as the European Union's Earth Observation Programme, Copernicus [20], and NOAA's Center for Operational

Oceanographic Products and Services, which is the authoritative US source for accurate, reliable, and timely tides, water levels, currents, and other coastal oceanographic and meteorological information [18].
- On a regional scale, e.g. focusing on the Mediterranean and other European Seas, there are several local forecast systems and services, such as WaveForUs [21], Poseidon [22], KASSANDRA Storm Surge System [23], Balearic Islands Coastal Ocean Observing and Forecasting System (SOCIB) [24], Coastal Observing System for Northern and Arctic Seas (COSYNA) [25], etc., usually covering ocean forecast needs on a national level.

The bulk of the aforementioned applications could significantly contribute to the rapidly expanding field of e-Navigation. However, these applications do not provide high-resolution sea level and wave climate forecasts at port scale, *i.e.* sea-state conditions adjacent to harbour protection structures inside port basins, rendering this discrepancy the main objective to tackle herein.

1.4. Scope of research

Within the Accu-Waves project [4] we currently develop a tool to provide fine resolution forecast data on prevailing sea states in the vicinity of ports and inside harbour basins [5]. The goal is to support navigation procedures of vessels' approach to ports. The basic decision support tool is developed in the form of a single software suite with inter-connected sub-codes, which is able to provide a reliable 3-day prognostic depiction of maritime conditions in ports and their surrounding areas with a 3-hour step. Related sea conditions refer to the following parameters:

(a) weather data: wind intensity/direction and atmospheric pressure at sea level;
(b) sea level elevation due to meteorological conditions and tidal effects, and respective ocean currents' intensity/direction;
(c) wind-induced wave characteristics (significant wave height, spectral peak period and main direction of wind waves propagation);
(d) swell characteristics (height, mean period and main direction of long oceanic waves);
(e) seiches characteristics in ports.

In this paper, we present recent developments of three robust numerical models for the integrated simulation of sea level variations, wave propagation and transformation in gulfs and coastal areas with port facilities. Model H (HiReSS) [26–31] is a 2-DH hydrodynamic (storm surge) model for the simulation of barotropic circulation and sea level variations, based on the depth-averaged shallow water equations (Section 2.1.1). Model A (TOMAWAC) [32–36] is a 3rd generation spectral model that simulates wind-induced irregular offshore wave fields on a triangular finite element mesh covering areas of a few dozens of Km^2 across port approaches (Section 2.1.2). Model B (WAVE-L) [37–39] is based on the hyperbolic mild-slope equation and it simulates the transformation of complex wave fields in harbours and coastal areas in the vicinity of ports with varying bathymetries (Section 2.1.3).

Main goal of this study is to develop new features of models H and B and formulate a model A setup in order to render them fully operational as an integrated ensemble of simulation software for high-resolution forecasts of sea level variations, depth-averaged currents, spectral and regular wave fields, in areas around and inside port basins. A second goal is to calibrate and validate all models against sea level and wave data from *in situ* observations by tide gauges of either available national hydrographic services [40] or our own field measurement operations, and from laboratory experiments of wave propagation and transformation at flume scales [41,42]. Moreover, the numerical algorithms of the hydrodynamic and wave models are fitted in an integrated modelling system suite for automated operational forecasting of wave characteristics, surge-induced and tidal sea levels in and around significant ports of the Mediterranean Sea [5]. Expansion of application to 50 important ports worldwide is ongoing and set as an ultimate research goal. The final product is consisted by maps and high-resolution datasets of sea levels and wave disturbance characteristics for 3-day forecasts useful for navigation around and inside ports.

2. Methodology

The operational forecast implementation is based on the following steps

(a) Adaptation of three hydrodynamic numerical models;
(b) Calibration, testing, and integration of the models into a single suite;
(c) Implementation of the above suite to 8 ports in the Mediterranean Sea;
(d) Adaption of the forecast application in the operational MarineTraffic platform [96] providing wind, wave, sea level and current data at 3-h intervals for 3-day forecasts.

Model B tackles high-resolution wave propagation and transformation inside harbour areas, while model A provides wave boundary conditions to model B, with model H contributing input data of sea levels and mean currents to both models A and B.

2.1. Numerical models

2.1.1. Model H: HiReSS

High Resolution Storm Surge (HiReSS) numerical model is built on a Fortran code, developed in the Laboratory of Maritime Engineering in Aristotle University of Thessaloniki [27,43]. Model H simulates the 2-DH barotropic mode of hydrodynamic circulation in large water bodies, enclosed seas, gulfs and coastal areas over a rather shallow continental shelf, based on the shallow water equations [44,45]. Thus, model H can predict the elevation of sea level (Sea Surface Height; *SSH*) and the depth-integrated sea currents (induced by atmospheric forcing; wind and pressure) [46]. HiReSS can take into account the combinatory effects of several processes, such as the inverse barometer (response of sea level to atmospheric pressure gradient of large barometric systems); shear stresses of wind applied on the air-water interface; geostrophic Coriolis forces on large water masses; astronomical tides; ocean bottom friction; turbulence of horizontal vortices through the eddy viscosity concept; impacts of the wave-induced mean flows (Stokes drift) on the wind-driven currents in open seas; additional sea surface set-up caused by wave breaking in nearshore coastal zones. Therefore, model H can reproduce the variations of sea level (*i.e.* positive or negative surges), ranging from decimeters to a few meters and lasting from several hours to a few days. The main advance of the HiReSS model is the tidal signal parameterization in the Navier-Stokes equations. The extended continuity and momentum equations, in order to account for meteorologically driven and tidally affected circulation can be written as:

$$\frac{\partial \zeta}{\partial t}+\frac{\partial Uh}{\partial x}+\frac{\partial Vh}{\partial y}=0 \tag{1}$$

$$\frac{\partial U}{\partial t}+U\frac{\partial U}{\partial x}+V\frac{\partial U}{\partial y}-f_C V+Z_x=-\frac{1}{\rho_o}\frac{\partial P_A}{\partial x}+E_h\left(\frac{\partial^2 U}{\partial x^2}+\frac{\partial^2 U}{\partial y^2}\right)+\frac{C_s}{\rho_o}\frac{W_x\sqrt{W_x^2+W_y^2}}{(d+\zeta)}-C_b\frac{U\sqrt{U^2+V^2}}{\rho_o(d+\zeta)} \tag{2}$$

$$\frac{\partial V}{\partial t}+U\frac{\partial V}{\partial x}+V\frac{\partial V}{\partial y}+f_C U+Z_y=-\frac{1}{\rho_o}\frac{\partial P_A}{\partial y}+E_h\left(\frac{\partial^2 V}{\partial x^2}+\frac{\partial^2 V}{\partial y^2}\right)+\frac{C_s}{\rho_o}\frac{W_y\sqrt{W_x^2+W_y^2}}{(d+\zeta)}-C_b\frac{V\sqrt{U^2+V^2}}{\rho_o(d+\zeta)} \tag{3}$$

$$Z_x=0.9g\frac{\partial \zeta}{\partial x}-0.7g\frac{\partial \zeta_{tide}}{\partial x},\qquad Z_y=0.9g\frac{\partial \zeta}{\partial y}-0.7g\frac{\partial \zeta_{tide}}{\partial y} \tag{4}$$

where ζ is the free surface elevation in the continuity equation (Eq. 1) yielding values of *SSH;* $h=d+\zeta$ is the total water depth of the sea and d is the local still water depth; U and V are the depth-integrated horizontal velocity components along the x and y axes of an ortho-regular staggered Cartesian grid of the Arakawa-C type for the Finite Difference Method (FDM); t is the time; f_C is the Coriolis coefficient; g is the acceleration of gravity; P_A is the atmospheric Sea Level Pressure (*SLP*); ρ_o is the average seawater density; C_b is the bottom friction coefficient following a logarithmic wall-law on the bed boundary layer [26,47] and C_s is the air-water drag coefficient [26,48]; W_x and W_y are the wind velocity components at 10 m above Mean Sea Level (MSL); E_h is the horizontal eddy viscosity coefficient for internal friction forces is based on a Smagorinsky-type of approach [26,29].

The boundary conditions of *SSH* or current velocities on the unique open boundary (*i.e.* the Gibraltar strait) of the Mediterranean domain are implemented via a Dirichlet-type approach (*a priori* known values of parameters), *e.g.* $\zeta=\zeta_{tide}(t)$, from a simplistic static model for astronomical tides (see below) or automated forecasts from established databases [20]. The boundary conditions of *SSH* or current velocities on the coastal solid boundaries are based on the approximation of irregular flow and are of the Von Neumann type (a priori known boundary-adjacent variable gradient) [49]. The chosen numerical scheme of integration is an explicit "leap-frog" algorithm with small time step $dt \approx 30$ s, in order to keep a sufficiently low Courant number.

Model H also takes into account the effects of astronomical tides on barotropic circulation (Z_x and Z_y terms of Eqs. (2)–(4)) through a static model parameterization [50], following a formulation that combines the equilibrium tidal potential with the self-attraction/loading effect under specific coefficient parameterizations [51,52]. Tide forecasts are based on the solution of harmonic equation ζ_{tide} on all grid cells with discrete longitudes and latitudes, concerning both semi-diurnal and diurnal tidal range signals [46]. Forecast of the tidal oscillation signal is based on the solution of a harmonic equation, which immediately applies the tidal balance budget (or potential of astronomical tide generation) by using the numerical series of Schureman [53] with equations of partial tidal harmonics:

$$\zeta_{tide}=\sum_{\nu}\zeta_{tide,\nu}(\lambda,\varphi,t)\begin{Bmatrix}\zeta_{tide,2}=k_o\sin^2(\varphi)\cos(\sigma_t t+x+2\lambda), & \nu=2\\ \zeta_{tide,1}=k_o\sin(2\varphi)\cos(\sigma_t t+x+\lambda), & \nu=1\\ \zeta_{tide,0}=k_o\left(3\sin^2(\varphi)\right)\cos(\sigma_t t+x), & \nu=0\end{Bmatrix} \tag{5}$$

Specifically, the second one ($\nu=2$) corresponds to the semi-diurnal tidal signal (*e.g.* M2 principal lunar mode), the third one ($\nu=1$) to the diurnal tidal signal (*e.g.* P1 principal solar mode) and the fourth one ($\nu=0$) to the long-period species of tidal signals; t is the Universal Standard Time (UST), λ and φ the geographic spherical coordinates, ζ_{tide} is the oceanic total tide amplitude, k_o is the magnitude of the partial tide, σ_t is the identical cyclic frequency of the partial tidal amplitude, and χ is the astronomical argument for every partial tidal budget (half range between high and low waters) in relation to midnight zero at the Greenwich meridian (00:00 Greenwich Mean Time, GMT). The major constants and values of all the

Table 1
Values of parameters and constants of the major tidal modes (harmonics of the eigenmodes of tidal oscillations) in model H.

Symbol of Harmonic Constituent	Tidal Oscillation Eigen-mode	k_o (m)	σ_t (10^{-4}/sec)	T (hrs)	χ (°)	Type of Tide
M2	Principal lunar	0.242334	1.10519	12.42	$2h_o$-$2s_o$	Semi-diurnal
S2	Principal solar	0.112841	1.45444	12.00	0	ν=2
N2	Elliptical lunar	0.046398	1.37880	12.66	$2h_o$-$3s_o$+p_o	
K2	Declination luni-solar	0.030714	1.45842	11.97	$2h_o$	
K1	Declination luni-solar	0.141565	0.72921	23.93	h_o+90	Diurnal ν=1
O1	Principal lunar	0.100514	0.67598	25.82	h_o-$2s_o$-90	
P1	Principal solar	0.046843	0.72523	24.07	h_o-90	
Q1	Elliptical lunar	0.019256	0.64959	26.87	h_o-$3s_o$+p_o-90	
Mf	Fortnightly lunar	0.041742	0.053234	327.86	$2s_o$	Long Period
Mm	Monthly lunar	0.022026	0.026392	661.30	s_o-p_o	ν=0
Ssa	Semiannual solar	0.019446	0.003982	4382.89	$2h_o$	

basic components of tidal modes are presented in Table 1. The mean longitudes of the sun and moon and the lunar perigee, h_o, s_o, at Greenwich midnight are also given by:

$$\begin{aligned} h_o &= 279.69668 + 36000.768930485T_d + 3.03 \cdot 10^{-4}{T_d}^2 \\ s_o &= 270.434358 + 481267.88314137T_d - 0.001133{T_d}^2 + 1.9 \cdot 10^{-6}{T_d}^3 \\ T_d &= (27392.500528 + 1.0000000356D)/36525 \\ D &= day + 365 \cdot (yr - 1975) + \text{int}[(yr - 1973)/4] \end{aligned} \tag{6}$$

where *day* is the number of day per year (*day*=1 on January 1st), *yr* is the year of study from 1975 and on, and int[] is the sign for the integer function of a number.

2.1.2. Model A: TOMAWAC

TELEMAC-based Operational Model Addressing Wave Action Computation (TOMAWAC) [32] is an open-source code for a 3rd generation, phase-averaged, directional, spectral wave model, developed by Électricité De France R&D's Laboratoire National d'Hydraulique et Environnement [33,34]. It simulates the evolution in space and time of the spectrum of sea surface elevation in waters of any depth. The numerical calculations are executed by the Finite Elements Method over an unstructured mesh. It is noted that the size ratio of the largest to the smallest computational element can exceed a value of 100, so TOMAWAC is also suitable for both offshore and nearshore applications, where high computational resolution is required. The model captures processes of wind wave generation and propagation; energy dissipation due to white-capping, bottom friction, wave shoaling and depth-limited breaking; non-linear triad and quadruple wave–wave interactions, wave-structure interaction (diffraction), wave-current interaction [54]. The main equation used by TOMAWAC for the evolution of the directional spectrum of the wave action density N is as follows, written in the form of a radiative transfer equation [55]:

$$\frac{\partial N}{\partial t} + \frac{\partial (\dot{x}N)}{\partial x} + \frac{\partial (\dot{y}N)}{\partial y} + \frac{\partial \left(\dot{k}_x N\right)}{\partial k_x} + \frac{\partial \left(\dot{k}_y N\right)}{\partial k_y} = Q(k_x, k_y, x, y, t) \tag{7}$$

$$\dot{x} = \frac{C_g k_x}{k} + U_x, \;\; \dot{y} = \frac{C_g k_y}{k} + U_y, \quad \dot{k}x = \frac{\partial \sigma}{\partial d}\frac{\partial d}{\partial x} - k\frac{\partial U}{\partial x}, \dot{k}Y = \frac{\partial \sigma}{\partial d}\frac{\partial d}{\partial y} - k\frac{\partial U}{\partial y} \tag{8}$$

where $k = 2\pi/L$ is the wavenumber, L is the wave length, $\mathbf{U} = (U_x, U_y)$ with $U = |\mathbf{U}|$ is the transport rate velocity and its components through geographic and spectral space (x, y and σ, d respectively) derived using the linear wave theory, C_g is the relative (or intrinsic) group celerity of waves (as observed in a moving frame of reference), C=σ/k the wave celerity, σ the cyclic frequency, and Q is an ensemble of source terms accounting for the generation and dissipation of waves due to all aforementioned wave processes [56]. Further details are described analytically in TOMAWAC user manual [57].

The numerical solution is done on a planar 2-D computational domain (for water areas) built upon a triangular mesh. The mesh-based discretization technique inherently allows for variability of cell sizes particularly facilitating resolution refinement in areas with complex geometries (gulfs, straits, bays, port approaches, coastlines, etc.) and rapidly diverging bathymetries. The user-defined density of spatial discretization points is always chosen to match the spatial scale of variation of the bathymetry, as the forcing input of wind fields is rather crude in terms of resolution. TOMAWAC's solver deals with a transport (convection-type) equation (Eqs. (7) and (8)) with source terms, that leads to the calculation of four-variable functions on a 4-D mesh in spherical or Cartesian coordinates, angle and frequency domain (φ, λ, θ, f) corresponding to a transport vector. TOMAWAC's solver uses a fractional step method, *viz.* the two steps of convection and source term integration are completed in a successive way. The convection step is treated by the Method of Characteristics (MoC; piecewise ray method). In case diffraction is not taken into account and the water depth is constant over time, the characteristics have to be traced

only once, at the beginning of the computation. This makes the propagation scheme very fast and efficient. The source term integration is carried out through a semi-implicit scheme [58].

2.1.3. Model B: WAVE-L

The WAVE-L model [37,39] is based on the 2-DH, depth-integrated, harmonic, hyperbolic formulation of the mild-slope equation for wave propagation [59]. It is a phase-resolving wave model and simulates regular or quasi-regular wave propagation in coastal waters of mildly sloping beds [60]; it resolves processes of wave-current interaction, wave shoaling, refraction, diffraction, wave reflection at solid boundaries, energy dissipation due to bottom friction, and depth-induced wave breaking in a combinatory way [38,61]. The numerical solution of the equations is based on an explicit scheme applied on a grid staggered between the cell values of surface elevation and mean velocities. Along the open sea and lateral boundaries sponge layers are used.

The basic equations for mass and quantity of motion conservation can be derived by replacing both pressure and velocity distributions that correspond to linear theory (for small amplitude waves) in the linearized Navier-Stokes equations (valid for periodic wave propagation from deep to shallow waters). Thus, for numerical simulations of wave transformation in 2-DH (depth-averaged) formulation, the continuity and momentum equations can be written as:

$$\frac{\partial \eta}{\partial t} + \frac{\partial (U_w d)}{\partial x} + \frac{\partial (V_w d)}{\partial y} = 0 \tag{9}$$

$$\frac{\partial U_w}{\partial t} + \frac{1}{d}\frac{\partial \left(c^2 \eta\right)}{\partial x} - \frac{1}{d}\frac{g\eta}{\cosh(kd)}\frac{\partial d}{\partial x} = v_h \frac{\partial^2 U_w}{\partial x^2} + v_h \frac{\partial^2 U_w}{\partial y^2} - f_b \sigma U_w \tag{10}$$

$$\frac{\partial V_w}{\partial t} + \frac{1}{d}\frac{\partial \left(c^2 \eta\right)}{\partial y} - \frac{1}{d}\frac{g\eta}{\cosh(kd)}\frac{\partial d}{\partial y} = v_h \frac{\partial^2 V_w}{\partial x^2} + v_h \frac{\partial^2 V_w}{\partial y^2} - f_b \sigma V_w \tag{11}$$

where η is the wave-induced free-surface elevation, U_w and V_w are the depth-integrated horizontal (wave-driven) velocity components along the x and y axes, respectively, c is the wave (phase) celerity, $\sigma = 2\pi/T$ is the wave angular frequency, f_b is the normalized bed friction coefficient, v_h is the horizontal eddy viscosity coefficient. The above equations result from the replacement of pressure and velocity distributions, from linear theory (for rather short waves), in the linearized Navier-Stokes equations, and thus provide the ability to describe transmission of simple harmonic undulations (monochromatic waves) at any depth. Extra terms for energy dissipation are further added and specialized modifications of the wave generation mechanism can also account for quasi-irregular wave propagation inside the computational domain.

Depth-limited wave breaking in shoaling areas, shallow waters, and even above submerged structures or alongshore bars, can be modeled in both monochromatic and pseudo-spectral waves' simulations using the eddy viscosity concept for Reynolds stresses that are expressed via a coefficient v_h in the r.h.s. of the momentum equations (Eqs. (10) and (11)) [62], where D defines the energy dissipation due to wave breaking [63], and coefficient Q_b can be derived, based on the Rayleigh distribution assumption for wave trains in nearshore areas, from the equations:

$$v_h = 2h\left(\frac{D}{\rho}\right)^{1/3} \tag{12}$$

$$D = \frac{1}{4} Q_b f_s \rho g H_m^2, \quad \text{where} \quad \frac{1 - Q_b}{\ln Q_b} = \left(\frac{H_{rms}}{H_m}\right)^2 \quad \text{for irregular waves} \tag{13}$$

$$D = \frac{1}{4}\rho g \frac{H^2}{T} \quad \text{or} \quad D = \frac{0.12 c_g}{h}\left(\bar{E} - \bar{E}_{st}\right) \quad \text{for monochromatic waves} \tag{14}$$

where f_s is the mean spectral frequency ($f_s = 1/T_m$, T_m mean spectral wave period), H_m is the maximum wave height with $H_m = \gamma d$, γ is the wave breaking parameter ($\gamma \approx 0.55$–1.0) for spectral waves, H is the regular wave height, T is the monochromatic wave period, overbar denotes mean values, $E = \rho g H^2/8$ is the wave energy, E_{st} corresponds to $H_{st} = 0.42 H_b$, $H_b = \gamma d$ is the regular breaking wave height, Q_b is the percentage of breaking waves at a particular depth d, and H_{rms} is the root-mean-square wave height $H_{rms} = 2(<2\eta^2>)^{1/2}$ and brackets $<\bullet>$ denote time-averaged values. It is inferred that for the total prevalence of breaking waves $Q_b = 1$ whereas for non-breaking waves $H_{rms} << H_m$, *i.e.* $Q_b << 1$. This modelling approach simulates breaking of random waves in complex bathymetries, conforming to the requirements of operational pseudo-random wave forecasts with model B.

Energy dissipation due to bottom friction is modeled using the linearized (normalized by local depth d) terms in the r.h.s. of the momentum equations (Eqs. (10) and (11)) in x- and y-directions of the Cartesian horizontal plane. The linearized bottom friction coefficient f_b is a function of the wave-induced velocity and the wave friction coefficient f_w, following the relationship:

$$f_b \sigma = \left(\frac{1}{2} f_w \sqrt{U_w^2 + V_w^2}\right)/d \tag{15}$$

In model B, the wave generation can be simulated on any longitudinal and lateral boundary simultaneously, with corresponding expansion of the peripheral sponge layers by an exponential damping factor of the wave energy content [64],

$DF(x)$ as:

$$\mathrm{DF(x)} = \exp\left[\left(2^{-\mathrm{x}/\Delta\mathrm{x}} - 2^{\mathrm{x_s}/\Delta\mathrm{x}}\right)\ln b\right], \quad 0 < x \le x_s \tag{16}$$

where x_s is the width of the sponge layer, b=1+r_s+exp(-1/r_s), where r_s=10/N_s and N_s is the number of grid points inside the sponge layer. This way, we are now capable to spatially restrict the computational field in areas adjacent to harbours and thus reduce demand of computational time and resources.

Monochromatic waves are generated along any boundary line by a sinusoidal excitation equation:

$$\eta_i^* = 2\frac{H}{2}\sin\left(\sigma\left(t - t_f\right)\right)\cos\varphi c\frac{\Delta t}{\Delta x} \tag{17}$$

where $t_f = \sin(\varphi) \bullet x/c$ and φ is the angle of incident wave direction. Moreover, the new version of model B is modified to simulate multi-directional, quasi-irregular waves (multiple frequency waves generated on the boundary, yet propagating with single group celerity). The generation and propagation of spectral waves may furthermore account for several different angles and directions simultaneously, practically following a modelling approach [65] that provides the directional spreading function $D(f,\theta)$ by the Fourier series representation for the wrapped normal spreading function [41], as:

$$\mathrm{D(f,\theta)} = \frac{1}{2\pi} + \frac{1}{\pi}\sum_{\mathrm{n=1}}^{\mathrm{N}}\exp\left[-\left(\frac{\mathrm{n}\sigma_\mathrm{m}}{2}\right)\right]\cos[\mathrm{n}(\theta - \theta_\mathrm{m})] \tag{18}$$

where N is the number of terms in the series, θ_m is the mean wave direction (0° or 45° in our test cases), and σ_m the directional spreading parameter (either 10° or 30° in our tests).

Partial and full reflection of incipient waves from harbour structures are modeled based on an updated version of the Karambas and Bowers [66] modelling approach of an extra dissipation term in the r.h.s. of the momentum equations Eqs. (10) and ((11)) inserting a turbulent eddy viscosity coefficient ν_γ:

$$\ldots \nu_\gamma\left(\frac{\partial^2 V}{\partial x^2} + \frac{\partial^2 V}{\partial y^2}\right), \quad \ldots \nu_\gamma\left(\frac{\partial^2 U}{\partial x^2} + \frac{\partial^2 U}{\partial y^2}\right) \text{ for the } x- \text{ and } y-\text{components} \tag{19}$$

where ν_γ is calculated via a system of complex equations (based on a complex wave number K) of the friction coefficient f_s, thus rendering them iteratively solvable for given values of the reflection coefficient C_R from literature.

If we assume that for a typical distance of $2S_w$ (S_w: structure width) the water depth in front of a solid boundary (breakwater, seawall, quay, etc.) is constant, and that the area of implementation of the coefficient ν_γ lies inside $0 \le x \le 2S_w$ with a full reflection applied exactly at $x = 2S_w$, for an incident wave with amplitude, a_i, and reflected amplitude, a_r, it follows [61]:

$$\eta = \alpha_i e^{i(\sigma t - kx)} + \alpha_r e^{i(\sigma t + kx)} \tag{20}$$

$$\sigma^2 - \nu_\gamma i\sigma K^2 = c^2 K^2 \tag{21}$$

where $\sigma^2 = gk\bullet\tanh(kd)$ (k=$2\pi/L$ being the wave length), and K is transformed into a complex number that satisfies the relation of Eq. (22). An analytical expression for C_r=$|a_i/a_r|$ can be finally derived as follows:

$$C_r = \left(\frac{\frac{K}{k}\left(1 + e^{-4iKS_w}\right) - \left(1 - e^{-4iKS_w}\right)}{\frac{K}{k}\left(1 + e^{-4iKS_w}\right) + \left(1 - e^{-4iKS_w}\right)}\right) \tag{22}$$

If the C_r value is known, the aforementioned system of equations can be solved with an approximation method and thus yield the value for the coefficient ν_γ. The reflection coefficient C_r for rubble mound breakwaters could be estimated from classic empirical relations in past literature, *e.g.* [67].

WAVE-L is a stable and robust model for the detailed simulation of wave propagation, within any port configuration, based on a Fortran code developed in the Laboratory of Maritime Engineering in Aristotle University of Thessaloniki (AUTh), rendering it an efficient tool to consider alternative scenarios of wave penetration in ports and wave agitation near coastal structures in harbours and marinas. The numerical solution of model B's equations is based on an established, explicit, validated scheme of FDM, which has been traditionally applied in numerical integration of long wave equations on a staggered orthogonal grid [68,69].

2.1.4. Model integration setup

The main steps taken to ensure an efficient set up of the operational simulations and the models' interactions are:

(a) The general mode of model H in the Accu-Waves framework (global mode) is forced using boundary and initial configuration data (if needed for ports in open sea areas) from the Copernicus Marine Environmental Monitoring Service (CMEMS) [20,70,71], and global-scale atmospheric input from NOAA [72]. The presented application for the Mediterranean Sea is forced by higher resolution (~10 km) meteorological simulations based on the Weather Research and Forecasting model with the Advanced Research dynamic solver (WRF-ARW, version 3.2.0) developed in AUTh [28,73–76].

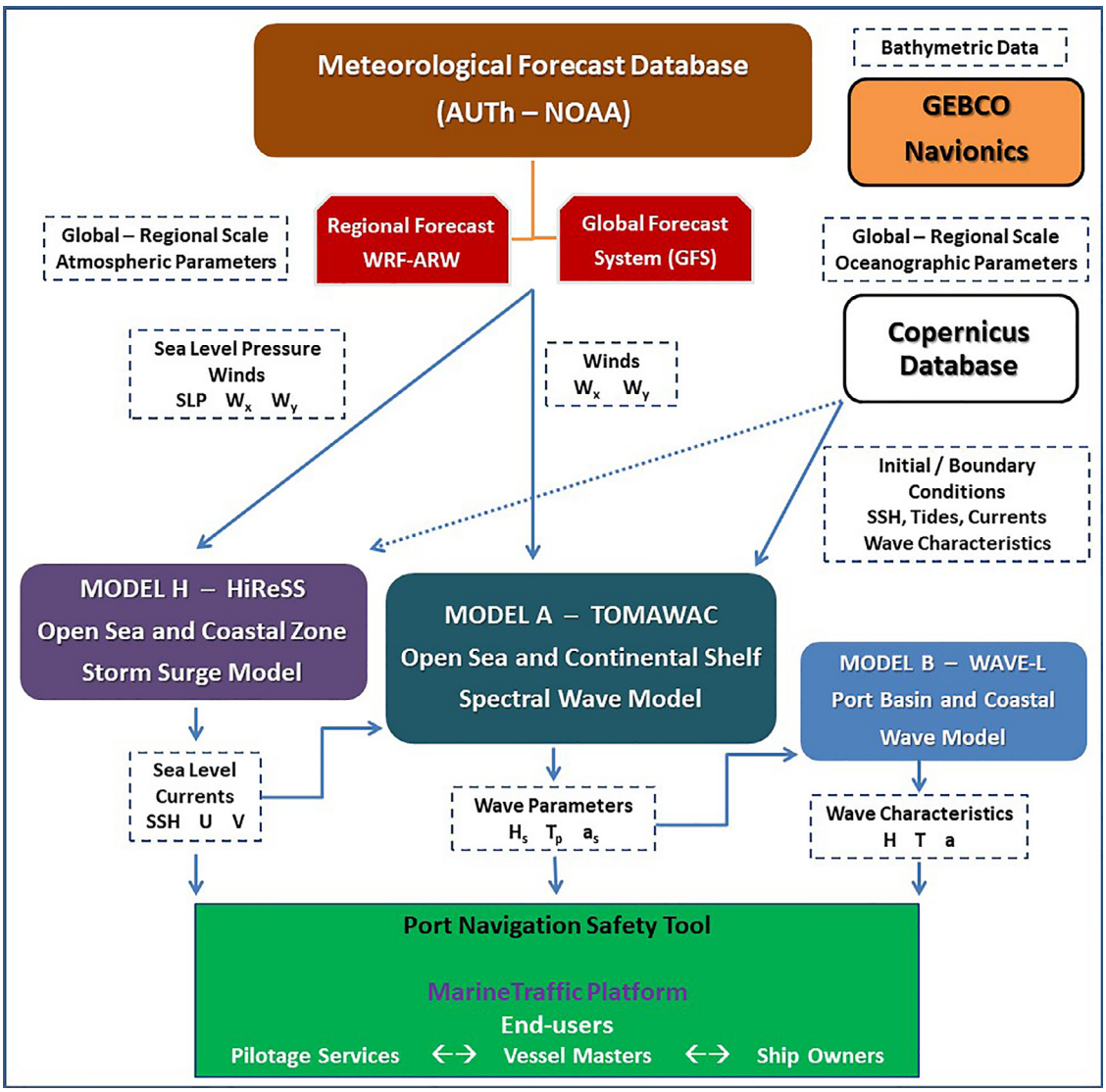

Fig. 1. Workflow diagram between high-resolution numerical models H, A and B forced by global/regional scale meteorological and oceanographic databases, and producing output for a Port Safety Management System. *SLP*: sea level pressure; W_x, W_y: wind zonal and meridional components; *SSH*: sea surface height; H_s: significant wave height; T_p: peak spectral period; a_s: mean spectral wave direction; H: regular wave height; T: monochromatic wave period; a: regular wave propagation direction.

(b) Model A is executed using spatial and temporal results of *SSH* and mean current speeds (*U, V*), in conjunction with data from the CMEMS database [77,78], concerning open-sea significant wave height (H_s), spectral peak wave period (T_p), and mean wave direction (a_p). The atmospheric forcing is the same as for model H. Information on the horizontal current velocity components and sea surface elevations obtained from model H are interpolated to model A's mesh to model the effect of wave-current interaction.

(c) Results obtained from model A in terms of H_s, T_p and a_p are extracted along the wave generation line of model B. It should be noted that the values of the aforementioned variables are extracted at coordinates that coincide with the cell centers of model B boundaries, to ensure compatibility and smooth interaction between the two models. Definitive bathymetry for model B execution is obtained by adding model H's *SSH* to *(d*.

In general, the three aforementioned numerical models tackle different needs in terms of area coverage and accuracy; schematics of the sequence of model interaction are provided in Fig. 1. The refined computational domain of model B is geographically nested to the coarser one by model A. The nesting techniques for model H output used as input in models A and B is based on a classic Wiener–Kolmogorov prediction algorithm for spatial analysis such as the linear or nonlinear Kriging method (depending on spatial complexity of the domain), *i.e.* by minimizing the variance of the error estimate ε

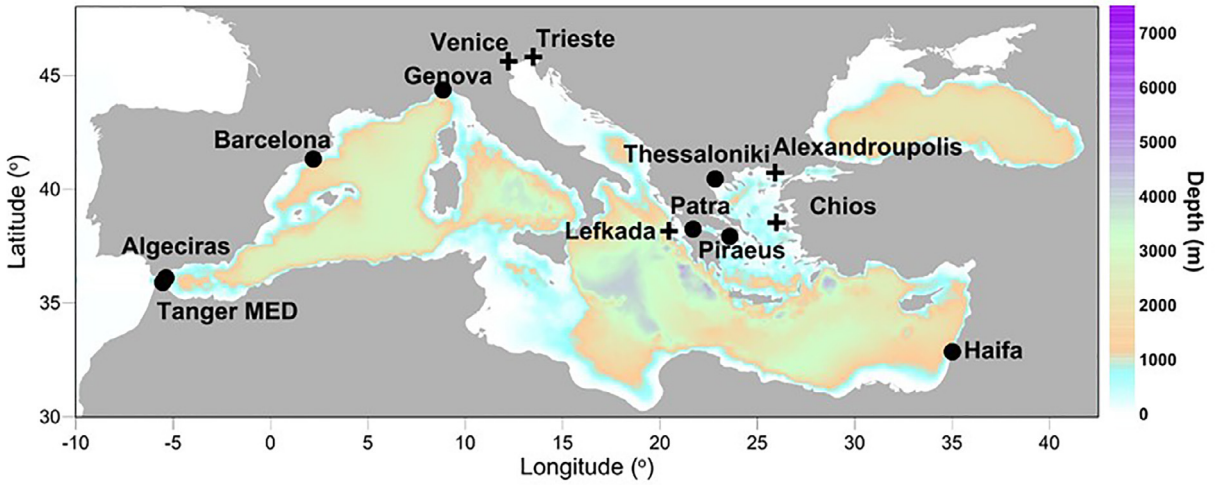

Fig. 2. Bathymetry chart of the Mediterranean Sea (including Black Sea; excluding Atlantic Ocean) referring to the computational domain (Level I) of model H from the GEBCO database with the locations of eight selected ports (black dots). Additional Mediterranean stations used for evaluation reasons are marked with a cross.

of a random variable Z (representing any scalar maritime parameter, as H_s or SSH) at a central point of interpolation x_0 as follows:

$$\varepsilon(x_0) = \hat{Z}(x_0) - Z(x_0) = \sum_{i=1}^{N} w_i(x_0) \times \mathrm{Z}(x_i) - Z(x_0) \tag{23}$$

where $i = 1,N$ is the number of assimilated/interpolated grid points and w_i are the individual spatial weights based on each point location compared to x_0. For the interpolation of vectoral parameters (*e.g.* currents *U, V*), the Nearest Neighbor algorithm is implemented.

2.2. Ports and maritime areas of application

The implementation of the operational integrated model suite concerns eight very important ports of the Mediterranean Sea, *i.e.* three Greek, two Spanish, and one Italian, Israelian, and Moroccan commercial harbours (Fig. 2). Nevertheless, the final outcome of the Accu-Waves initiative [4,5] will be to build a sea-state forecast application which is intended for 25 coastal regions globally, covering areas with complex bathymetries and diverse coastlines. These areas will contain in total 50 port facilities with high traffic load and significant commercial interest, serving international shipping operations. Bathymetric information in the relevant sea areas of the selected port sites were obtained through local services, as the Hellenic Navy Hydrographic Service (HNHS) [40], the Navionics platform [79], and the General Bathymetric Chart of the Oceans (GEBCO) database [80].

In general, model H is applied to much larger water bodies than the vicinity of a single port in order to capture large scale meteorological processes present over such broader areas (Table 2). Herein we present pilot implementations of model H in the Mediterranean Sea with 1/20° (almost 5 km) spatial resolution (Fig. 2). Results focus on the harbours of Algeciras and Barcelona in Spain, Genova in Italy, Haifa in Israel, Thessaloniki, Patra and Piraeus in Greece, and Tanger-Med in Morocco to provide crucial information of sea level predictions locally and input to models A and B in these areas.

Regarding model A (Table 2), *ad hoc* delineations of the sea area are performed, where environmental input data are sought from globally established met-ocean data sources (see Section 2.3). Overall expanse of interest around a port is defined as the water surface of a circular area centered at the port with a 3–45 km radius. Model A is one-way coupled to the coarser model H, covering maritime areas around ports of typically $\leq$2500 Km^2. For the case of swell dominated sea states, a modification of model A's spectral spreading parameter s is used to accurately take into account the long wave propagation [81].

Pilot implementation of model B is carried out in all Mediterranean ports (only the three largest Greek harbours shown herein for the sake of brevity). The high resolution of model B is based on Kriging interpolations of the finest available resolution bathymetric depth charts [40,79]. Model B is one-way coupled to the coarser model A for input boundary conditions; the port area of typically $\leq$10 Km^2 is integrated in larger domains. It also receives input of local changes in bathymetry from model H [31,39]. Model B's resolution corresponds to a very fine discretization step of $\Delta x \leq 2$ m inside the port basin, in order to appropriately resolve and describe waves with length $L \geq 10$ m.

Table 2
Basic parameterizations and main attributes of the wave and storm surge models (A, B and H).

Attribute / Parameterization	Implementation characteristics	
Hydrodynamic model	**HiReSS (Model H)**	**Shallow water equation for barotropic circulation and storm surge**
Regional Sea	Mediterranean basin	
Forcing / Driving field	NOAA and AUTh [72,73]	*SLP*, W_x, W_y products, 0.1° × 0.1°, 3-h
Spatial resolution / Domain	1/20° × 1/20°	Enclosed basin
Bathymetry	GEBCO [80]	Staggered grid Arakawa-C type
Simulation time span	3 days (72 h) with 3-h output	
Integration time step / Output	30 s	3-h
Free-surface / Bottom friction	Smith and Banke [48]	Wang [47]
Boundary / Nesting technique	Dirichlet / Open sea boundary with estimated free surface	
Eddy viscosity treatment	Boussinesq hypothesis: Smagorinsky model for horizontal eddies	
Tidal component approach	Static model by Schwiderski [50]	
Wave model	**TOMAWAC (Model A)**	**3rd generation phase-averaged spectral**
Gulfs, Bays, Local Seas	Thermaikos, Patraikos, Saronikos Gulfs, Gibraltar & Haifa Bay, Gibraltar Strait, Iberian & Ligurian Sea	
Forcing / Driving field	NOAA and AUTh [72–74]	W_x, W_y products, 0.1° × 0.1°, 3-hour
Initial / Boundary Conditions	CMEMS [20]	Copernicus MEDSEA ANALYSIS FORECAST WAV-006-017 products, 0.042° × 0.042°, 1-h
Spatial resolution / Domain	Varying: 50–500 m	Semi-enclosed gulfs
Bathymetry	Hydrographic Services [40,79]	Finite Elements [57]
Frequency range	0.04–1 Hz	0.056–1 Hz
Integration time step / Output	10 min	3-h
Integration scheme	MoC for propagation – Semi-Implicit for source terms [58]	
Wave model	**WAVE-L (Model B)**	**Hyperbolic mild-slope equation phase-resolving**
Ports	Algeciras, Barcelona, Genova, Haifa, Patra, Piraeus, Tanger Med, Thessaloniki	
Driving field	Model A results	H_s, T_p, a_p
Spatial resolution / Domain	Fixed: 2 m	Port approaches and harbour basins
Bathymetry	Hydrographic Services [40,79]	Staggered orthogonal grid [68,69]
Integration time step / Output	0.1 s	3-h
Wave breaking model	Eddy viscosity	Battjes and Janssen [62]
Boundary conditions	Sponge layer	Partial/Full reflection from structures [66]
Wave generation	Quasi-irregular waves	Lee and Suh [65]

3. Validation of numerical models

The evaluation of the models' performance is conducted by comparisons of simulation results with available field observations and experimental data. The validation parameters and skill scores refer to sea levels (model H) and characteristic wave heights (models A and B).

3.1. Field observations and experimental data

We performed field observations in the Thessaloniki port during autumn and winter of 2019 with the use of a Sea-Bird Electronics measuring instrument, namely SBE26 Seagauge Wave and Tide Recorder [82] (Fig. 3a). SBE26 combines nonvolatile flash-type memory with stable time-base and a high-frequency quartz hydrostatic pressure sensor to provide real-time data of wave and tide recordings of high accuracy. For tide and water level monitoring, the pressure sensor output was integrated to average out wave action with a fine time-resolution of one minute. The wave features records were based on burst sampling, with one sample per 0.25 s, *i.e.* giving a burst duration of almost 8.6 min for 2048 samples in every hour of the day. All calculations were performed with the use of a modular software package Seasoft for Waves [83], which provides all pre-deployment planning, communication setup and uploading of pressure data from the SBE26, separation of the uploaded data into separate wave and tide files, removal of local atmospheric barometric pressure from tide data, statistical analysis of spectral wave parameters, etc. [84]. The needed local, real-time, (atmospheric) barometric pressure data were provided by the local weather station of AUTh's Department of Meteorology and Climatology via their Meteorological Observations online service [73]. The wave burst data were processed to compute wave statistics, results from auto-spectrum analysis, statistics from surface wave zero-crossing analysis, thus producing the observed timeseries of spectral wave characteristics, and the relevant Fast Fourier Transform coefficients.

Fig. 3 presents depictions of the measuring equipment together with the chosen locations of *in situ* observations performed in the Thessaloniki port basin. Two sets of field data were retrieved:

(a) for tidal and sea level measurements during 30/09/2019 – 14/11/2019,
(b) for tidal, sea level and wave measurements during 12/12/2019 – 28/12/2019.

The water depth at the point of measurements was around 10 m for the first set of field recordings and around 12 m for the second set of *in situ* measurements. These types of instrumentation can produce data only for progressive waves.

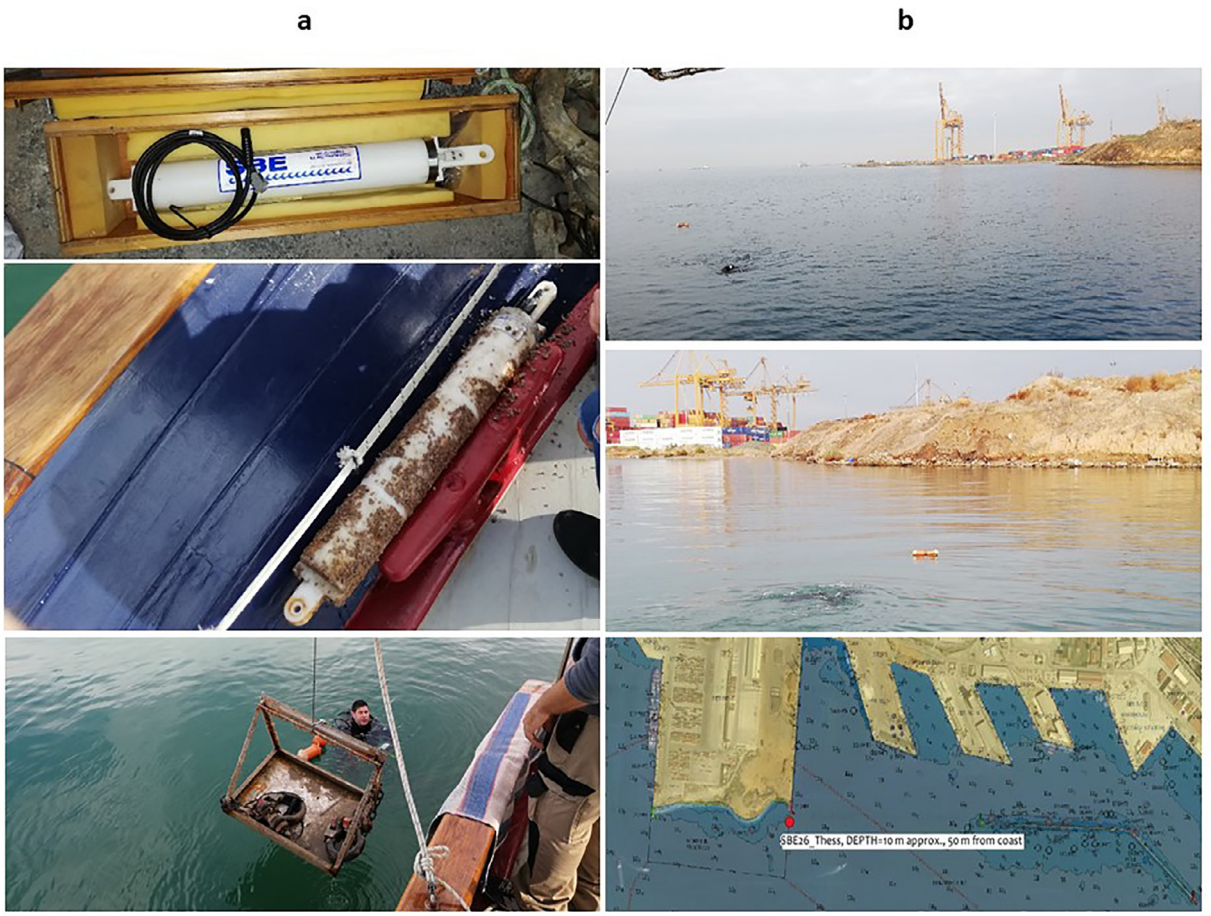

Fig. 3. Depiction of a) the SBE26 measuring instrument and its base-holder for field recordings of tides, sea levels, and wave features, b) the locations of *in situ* observations performed in the Thessaloniki port basin: approximately 22° 54.621' longitude, 40° 37.888' latitude.

Thus, for our case of a nearshore station and in order to avoid reflections from vertical structures and waterfronts in the port basin, we chose the location of SBE26 gauge immersion to be in front of a wave-dissipating beach-type formation with sloping bathymetry, *i.e.* ahead of the end (roundhead) of Pier 6 in Thessaloniki port (Fig. 3b).

Additional tide-gauge measurements of hourly- and daily-averaged *SSH* values were collected from available data sources. The Global Sea-Level Observing System (GLOSS) and Italian National Institute for Environmental Protection and Research (ISPRA) databases [85,86] provided sea level information for three Italian stations (Genova, Trieste and Venice; Fig. 2). Observational data from four Greek stations located in port basins (Alexandroupolis, Chios, Lefkada, and Thessaloniki; Fig. 2) were also obtained by HNHS [40]. Both datasets were retrieved in order to validate model H simulations. The recording periods correspond to 1995-2005 and 2012-2015. Values of *SSH* field observations were derived from measured data after subtraction of the MSL, determined by a post-processing heuristic technique of a high-pass filter with a cut-off frequency of 1/30 days. This was done in order to exclude long-term monthly oscillations of the sea level induced by steric effects [87] in the Mediterranean; these types of effects cannot be simulated by the 2-DH barotropic model H. Moreover, referring to long-term hindcasting storm surge climate runs (Section 3.2), model H did not include computation of the astronomical tides. For these cases the *SSH* tide-gauge data (at 4 Greek stations from 1995 to 2005) were de-tided using the T-Tide software [88].

The evaluation of model B's performance was conducted by comparisons of simulation results with experimental data of both regular and irregular wave propagation and diffraction around semi-infinite breakwaters and through breakwater gaps [42,89]. We also numerically reproduce an elliptical shoal experiment [41], concerning irregular incident waves, and therefore also test a directional pseudo-spectral wave generator for mild-slope equation wave models.

3.2. Model H validation

The HiReSS model has been applied in the past on a number of regions comprising large water bodies and marginal seas [45], and further calibrated and thoroughly validated via comparisons of hindcast modelling results against *in situ*

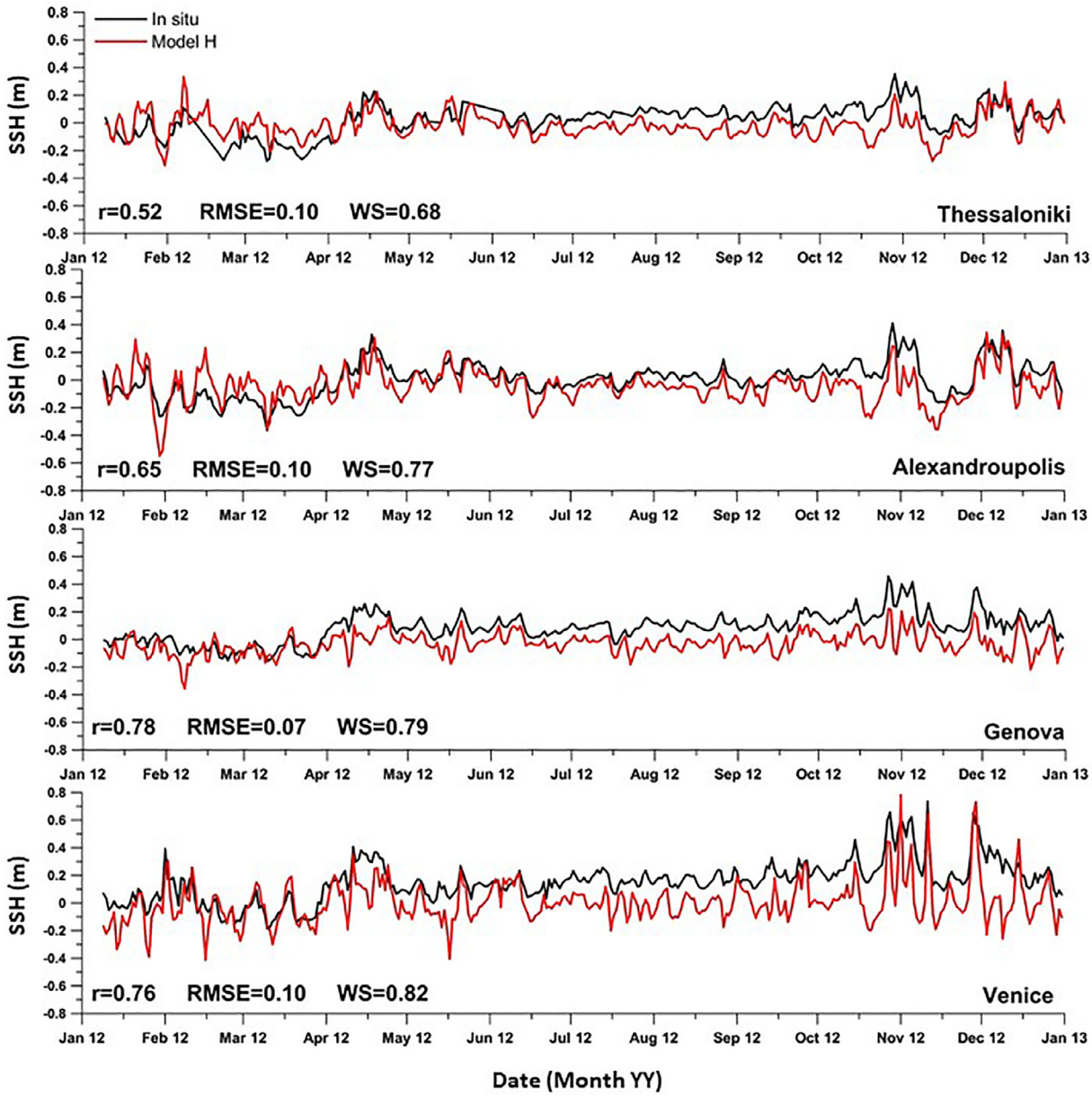

Fig. 4. Comparisons of model H hindcast results against *in situ* observations of *SSH* (m) by tide gauges, during 2012 in Thessaloniki, Alexandroupolis, Genova and Venice ports [40,85]. The following statistical measures are provided for quantitative validation; *WS*: Willmott Sill score; *RMSE*: root-mean-square error; *r*: Pearson correlation.

observations for either short periods with intense storm conditions [28,31] or large periods (> 15 yr; for extreme events of *SSH*) in the Mediterranean, Aegean and Ionian Seas to investigate the impact of climatic changes on the coast [26,29,30].

The daily-averaged simulated *SSH* time series (in hindcasting mode) provided by model H agrees well with the respective tide-gauge measurements during 2012 in the ports of Alexandroupolis, Thessaloniki, Genova and Venice (Fig. 4). For further quantitative evaluation of model H's performance the root-mean-square error (*RMSE*) is presented on the graphs, followed by the classic Pearson product-moment correlation coefficient *r*. Moreover, the Willmott Skill (*WS*) score or Index of Agreement [90] is also calculated for *SSH*. The higher the *WS* and *r* (with ≤ 1 as a limit), the better match is reached between simulated values of *SSH* and observations from tide gauges. High correlation coefficient values and prediction skills were achieved, *e.g.* $r = 0.52–0.78$ and $WS = 0.68–0.82$. Acceptable errors are also tracked reaching down to 12.8% of the occurred *SSH* maxima. It should be noted that the forecast skill of the storm surge model highly depends on the accuracy and resolution of the atmospheric forcing input [29,30,31]. A general ability of model H to capture high seas is confirmed. The latter is further corroborated by the results of Fig. 5, which portrays comparisons of *SSH* hindcasts with model H in Venice and Trieste, an

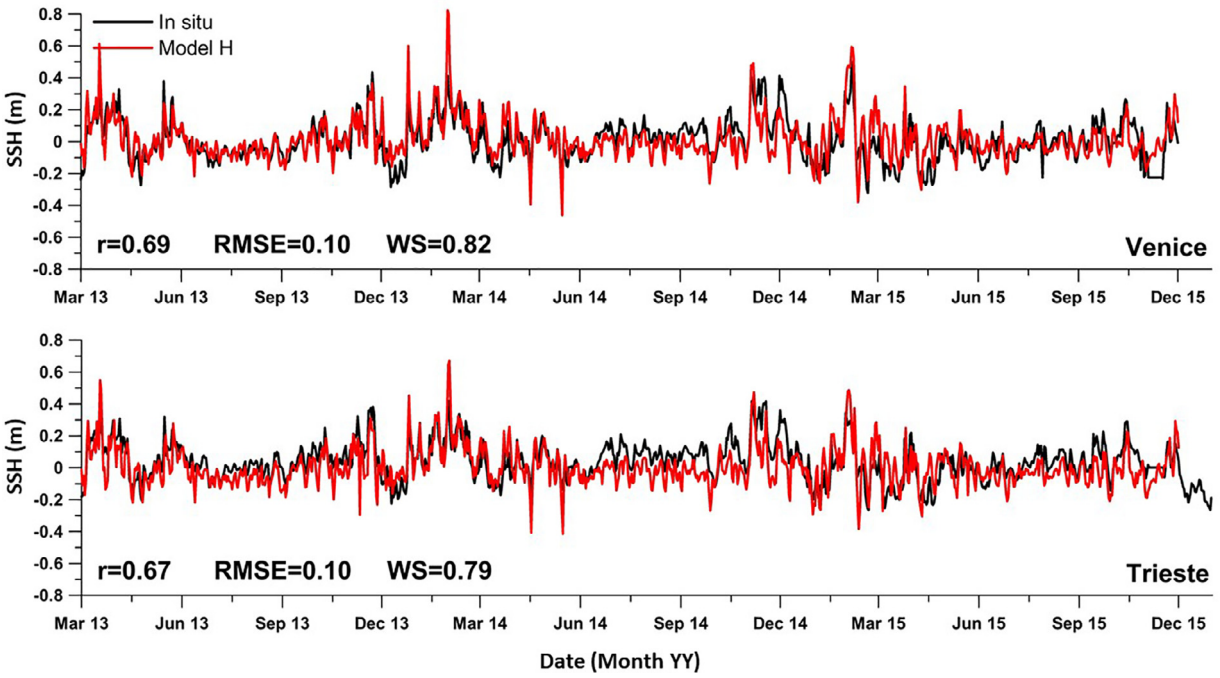

Fig. 5. Comparisons of model H hindcast results against *in situ* observations of *SSH* (m) by tide gauges [86], during 2013–2015 in Trieste and Venice ports. The following statistical measures are provided for quantitative validation; *WS*: Willmott Sill score; *RMSE*: root-mean-square error; *r*: Pearson correlation.

Table 3
Validation of model H long-term "climatic" hindcast results against *in situ* observations of *SSH* maxima (m) by tide gauges during 1995–2005 in 4 Greek ports. Statistical errors are provided for quantitative validation together with collective values for the Willmott Sill score *WS, RMSE*, Pearson correlation coefficient *r* and *HRP*-index.

Port Site	Mean E_i (%)	Mean EI_i	*HRP*-index
Thessaloniki	−6.29%	−0.206	0.98
Chios	8.28%	0.281	0.94
Alexandroupolis	−17.20%	−0.561	0.98
Lefkada	−4.17%	−0.133	0.95
AVERAGE	−0.05	−0.15	0.96
Overall skill factors at 4 Greek ports			
Pearson Correlation, *r*		0.841	
Root-mean-square error, *RMSE* (m)		0.026	
Willmott Skill score, *WS*		0.712	

area with extremely strong storm surge events [26], from 2013 to 2015. Good agreement is achieved between the modelled results and *in situ* observations of combined weather- and tide-induced sea level variations. Small discrepancies are found for large values of *SSH, i.e.* model H slightly overestimates the total sea level.

In order to further investigate the aforementioned discrepancy and thus evaluate model H's ability to capture characteristic values of *SSH* extremes, which are crucial to navigation and berthing in ports, we used the Storm Surge Index (*SSI*) [87] for comparisons of model and field data. *SSI* is calculated as the average of the three highest independent storm surge maxima per year; 5-day separated events were only considered referring to the estimated maximum duration of a Mediterranean storm [91]. Fig. 6 presents the evaluation of model H, based on comparisons of long-term hindcasting model results against *in situ* observations by tide gauges during 1995–2005 in four Greek ports (Fig. 2). Several statistical measures for inter-annual maxima of tidal-free *SSH* are compared, *i.e.* absolute SSH_{max}, *SSI*, and 99th percentile of *SSH*, together with the probability of occurrence of locally observed SSH_{max}. The comparisons support the generally efficient performance of model H, ranging from plausible to very good, with rather small errors for the 10-yr averages of *SSH* extremes. A tendency to sufficiently estimate the statistically significant high values rather than the absolute maxima, *e.g.* the 99th percentile in all stations, was also noticed. Errors range from miniscule, *e.g.* 4‰ in Thessaloniki and Chios ports for the 99th *SSH* quantile to 13% in Alexandroupolis port for the 10-yr extreme *SSH*. The probability of *SSH* local maxima occurrence is also well estimated by model H, indicating that it can capture the frequency of appearance of peaks in sea level elevation time series at coastal areas and ports [92,93].

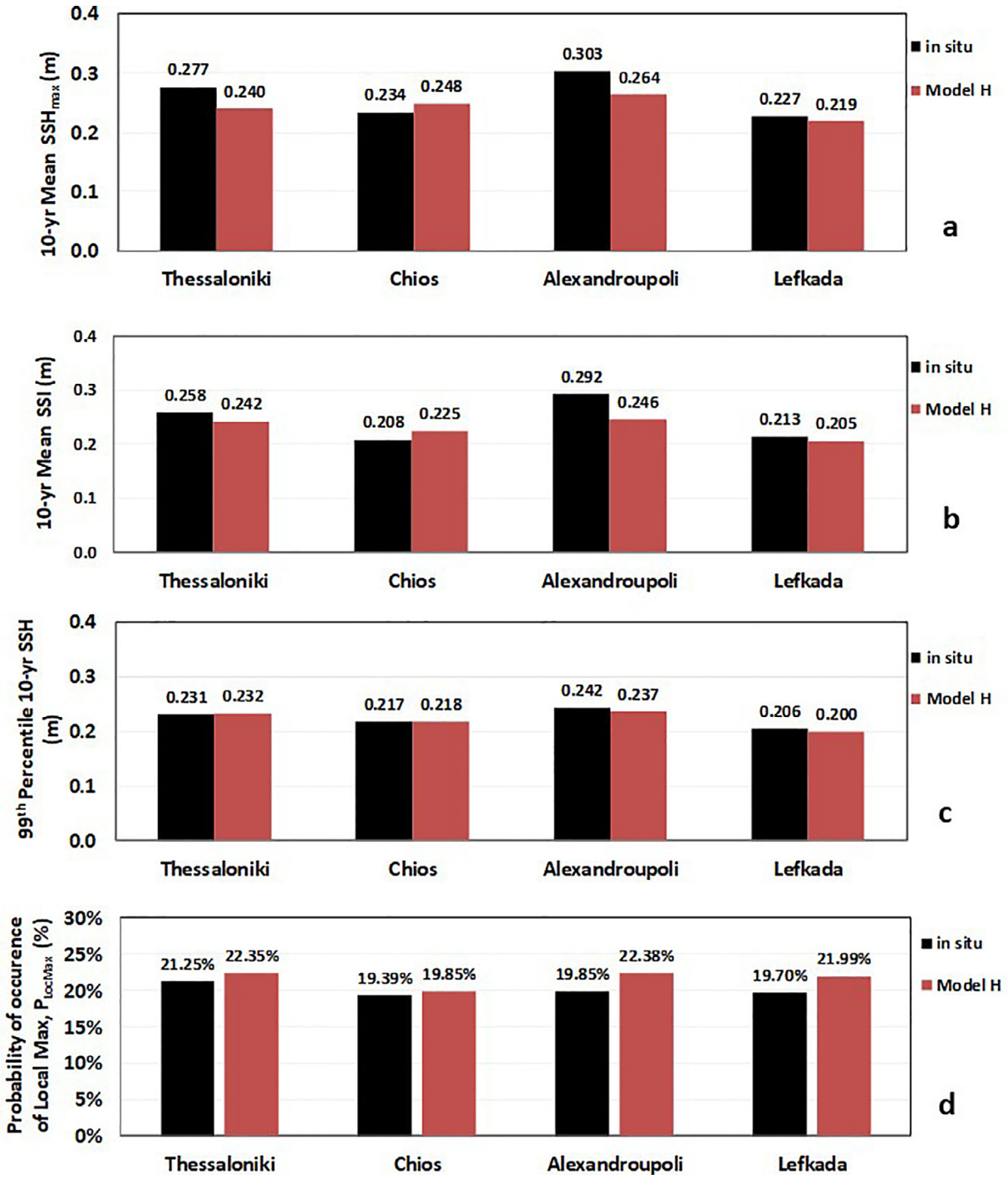

Fig. 6. Comparisons of model H long-term hindcasting model results against *in situ* observations by tide gauges during 1995–2005 in 4 Greek ports [40]. From top to bottom graph, the storm-induced sea level maxima are represented by the statistical measures: a) SSH_{max}, b) *SSI*, c) 99th percentile of *SSH* (m), and d) probability of occurrence of locally observed SSH_{max}.

As extra measures of comparison for model H's skill to reproduce sea levels, the corresponding Percent Error (E) and Error Index (EI), based on *SSI* values, were also calculated as:

$$E(\%) = 100 \cdot \left(\overline{SSI_{\text{mod}}} - \overline{SSI_{obs}}\right) / \left(\frac{\overline{SSI_{\text{mod}}} + \overline{SSI_{obs}}}{2}\right)$$

$$EI = \left(\overline{SSI}_{mod} - \overline{SSI}_{obs}\right) / \sqrt{\left(\sigma^2_{SSI_{mod}} + \sigma^2_{SSI_{obs}}\right)/2} \tag{24}$$

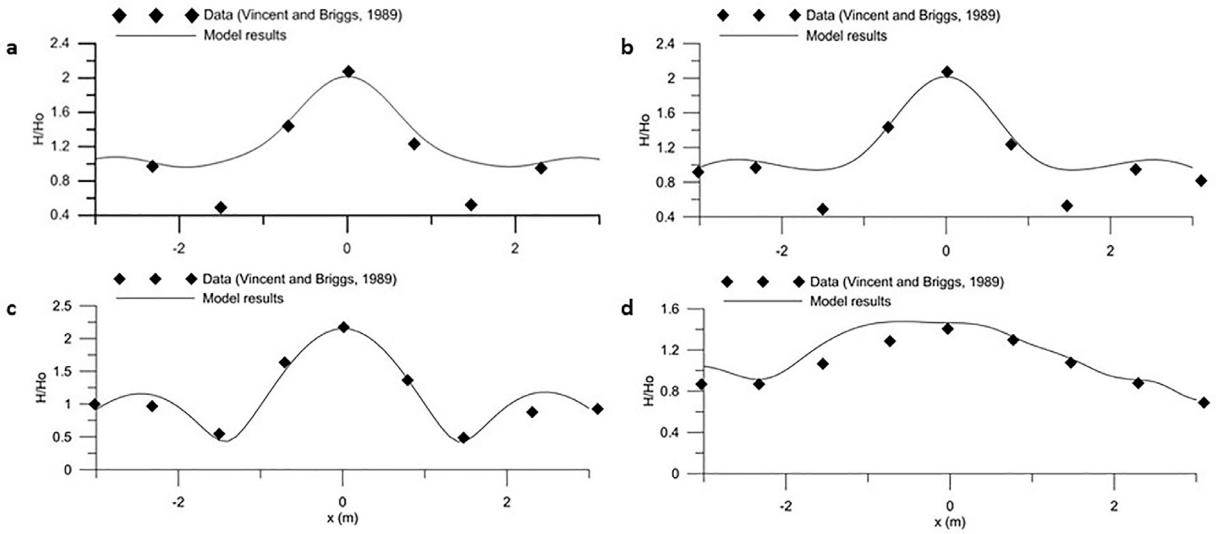

Fig. 7. Comparisons of model B results against experimental data [41], in terms of normalized wave height H/H_o, for spectral waves propagating over a circular shoal corresponding to experimental test cases a) U3, b) B3, c) M2 and d) N3 in [41].

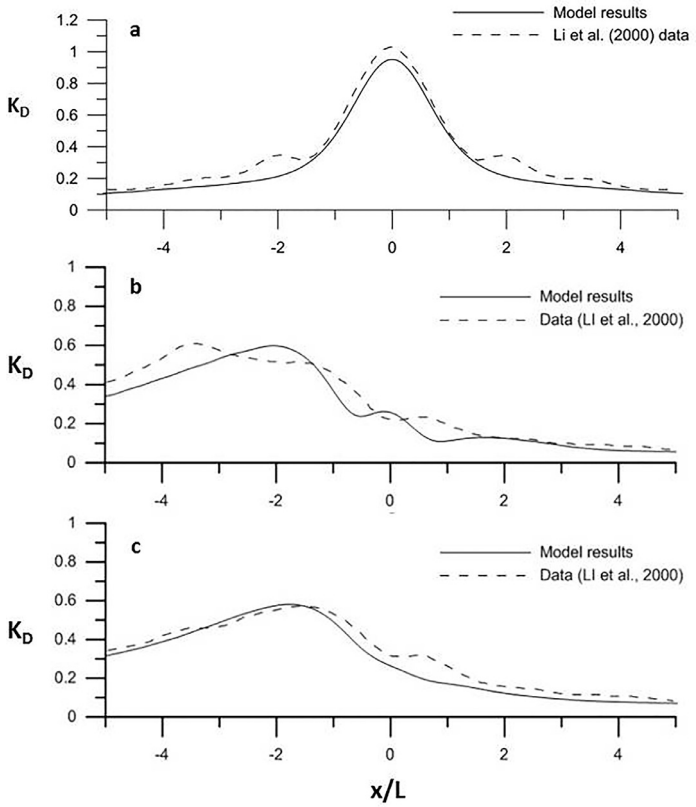

Fig. 8. Comparisons of model B results against experimental data [42,89], in terms of diffraction coefficient K_D for experimental data of: a) unidirectional quasi-irregular waves with spreading parameter $s=\infty$ and initial angle of propagation $\theta_o=90°$, b) multi-directional quasi-irregular waves with $s=19$ and $\theta_o=45°$, and c) unidirectional quasi-irregular waves with spreading parameter $s=\infty$ and initial angle of propagation $\theta_o=45°$.

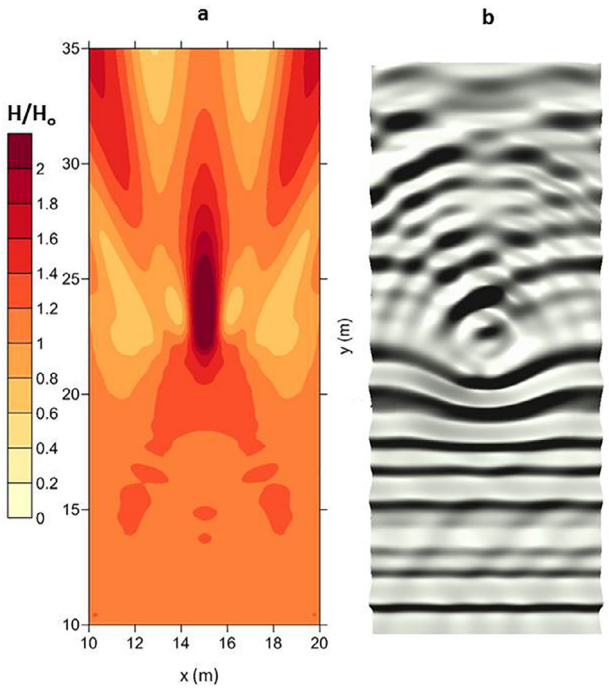

Fig. 9. Depiction of model B results for: a) normalized wave height H/H_o and b) wave-induced free surface elevation η, reproducing experimental data for unidirectional non-breaking spectral waves propagating over a circular shoal corresponding to experimental test case U3 in [41].

where the overbar denotes temporal averages, as derived from modelled ($_{mod}$) and observed ($_{obs}$) data, and σ_{SSI} is the standard deviation of the inter-annual variability of *SSI* time series for each station. *E* and *EI* turn positive when there is model overestimation of the sea level elevation over the field values. Furthermore, we calculated the Hit-Rate-of-Percentiles (*HRP*) index [94] for the entire 10-year *SSH* time series, in order to examine if bias correction is necessary for modelled storm surge results. *HRP*-index is calculated as the sum of the categorical fractions, *i.e.* differences between the sorted (from 1st to 99th) percentiles of simulated and observed values of *SSH*, compared to an allowed deviation. The latter was taken equal to half the average standard deviation of the modelled and *in situ SSH* time series, *i.e.* $(\sigma_{SSHmod}+\sigma_{SSHobs})/2$ that is 5-10% of average observed SSH_{max}. Model H was found to score higher than the limit of 0.95 in average and reached the value of 0.98 at the Thessaloniki port station. Therefore, bias correction was not considered necessary for forecasts of *SSH*.

Table 3 presents collective evaluation by statistical skill scores of model H for the long-term climatic hindcast results against tide-gauge observations of *SSH* maxima during 1995–2005 in four Greek ports. The largest simulation error (yet acceptable, $EI \approx -0.561$) is traced in Alexandroupolis station where, however, the *HRP*-index is quite high denoting good reproduction of the statistical distributions of *SSH* time series. In Thessaloniki port, the skill scores are high with low errors ($E < 7\%$). Overall skill factors at the aforementioned Greek ports reveal a high average correlation ($r = 0.841$) with low $RMSE = 0.026$ m, and appreciable $WS = 0.712$.

3.3. Wave models A and B validation

The TOMAWAC wave model has been used extensively for wave propagation and coastal engineering studies for over 20 years and thorough validations of the model with experimental and field data has been conducted [33–35,95]. For a detailed overview of the validation procedure for the TOMAWAC wave model the reader should refer to the above. In this paper, we focus on fundamental validation only for models H and B, which were created by members of our research team. Nonetheless, we present validation of operational runs of models A and B in Section 3.4.

Model B is based on the WAVE-L code which has also been applied at various coastal areas in the past, especially for the design of real-life harbour projects. Extensive validation via comparisons of modelling results against experimental data [96] referred to monochromatic wave propagation and refraction over an elliptic shoal on a 1:50 plane sloping seabed [61].

Hereby, an elliptical shoal experimental setup with a directional spectral wave generator [41] is also numerically reproduced with model B as a test of quasi-irregular propagation over an uneven bottom. The numerical wave flume is 35 m wide and 29 m long with a constant water depth of 0.46 m. The elliptical shoal has axes of 10.5–11.3% of the flume dimensions with its tip at 0.3048 m from the seabed. The wave period *T* of the incident waves (T_p for spectral waves) is 1.3 s and representative wave height *H* (H_s for irregular waves) is 2.54 cm. Fig. 7 presents satisfactory comparisons of model results

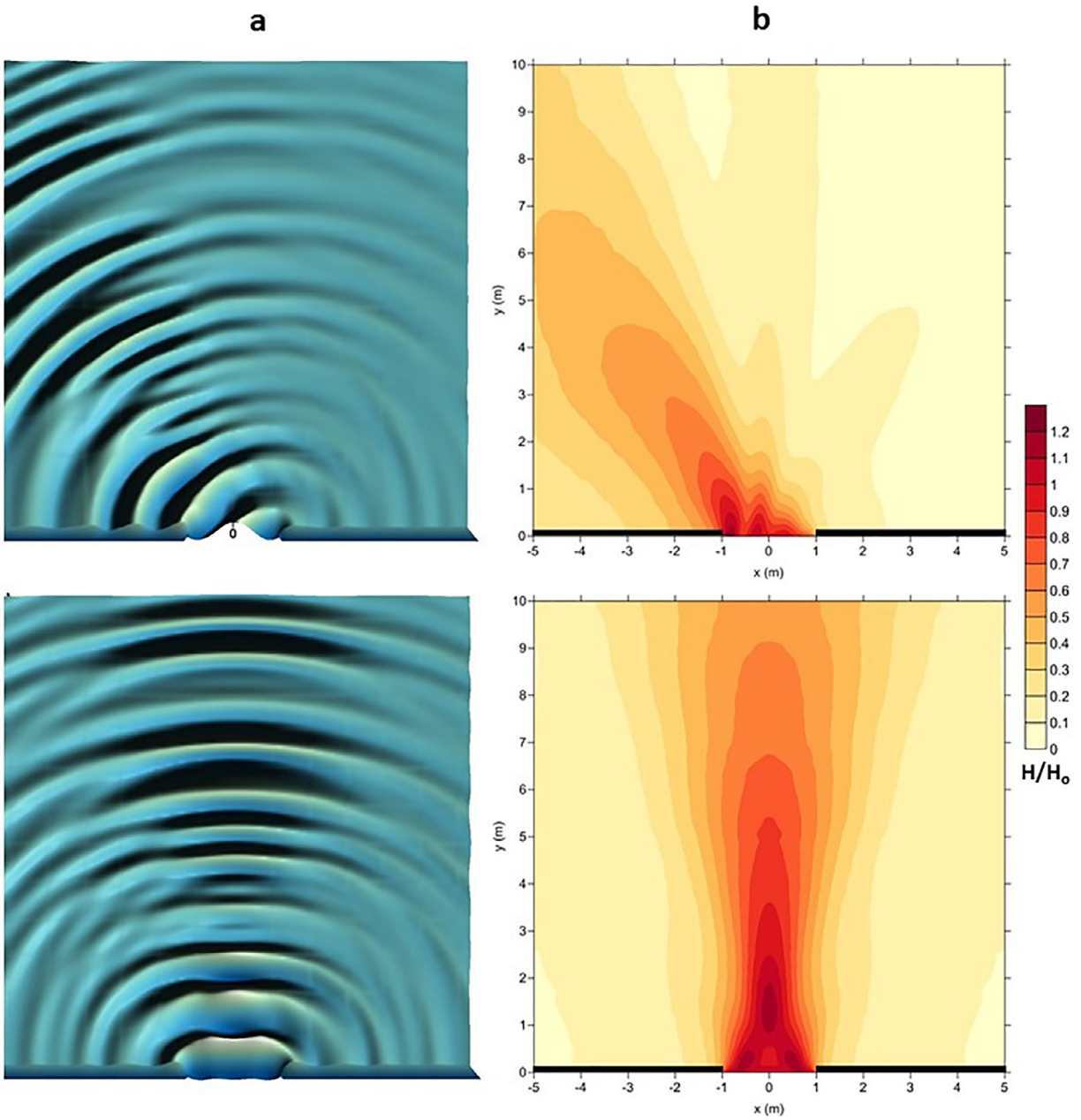

Fig. 10. Depiction of model B results for: a) the wave-induced free surface elevation η and b) the normalized wave height H/H_o, reproducing experimental data [42,89] for uni-directional irregular waves propagating and diffracted through a breakwater gap corresponding to a spreading parameter $s=\infty$ and initial angle of propagation $\theta_o=45°$ (upper graphs) and $\theta_o=90°$ (lower graphs).

against experimental data of both implementations, in terms of normalized wave heights H/H_o, where H_o is the offshore wave height. Tests refer to several experimental cases U3, B3 and N3 (non-breaking spectral waves), and M2 (non-breaking monochromatic waves) of [41], at various different transects of the shoal. Pearson correlations are quite high ($r > 0.9$), with rather low *RMSE* (ranging from 0.01 to 0.254 for H/H_o), giving a 5‰ minimum to a 12% maximum deviation from experimentally available maximum H/H_o ratio. In general, the comparisons show a good agreement between the model results and the experimental for narrow-banded directional spectra. Fig. 9 depicts model B results for the normalized wave height H/H_o and the wave-induced free surface elevation η, reproduced for the said experiment, referring to unidirectional non-breaking spectral waves over the shoal (test case U3); 2-DH distribution patterns of H_s and η is plausible compared to their experimental equivalents.

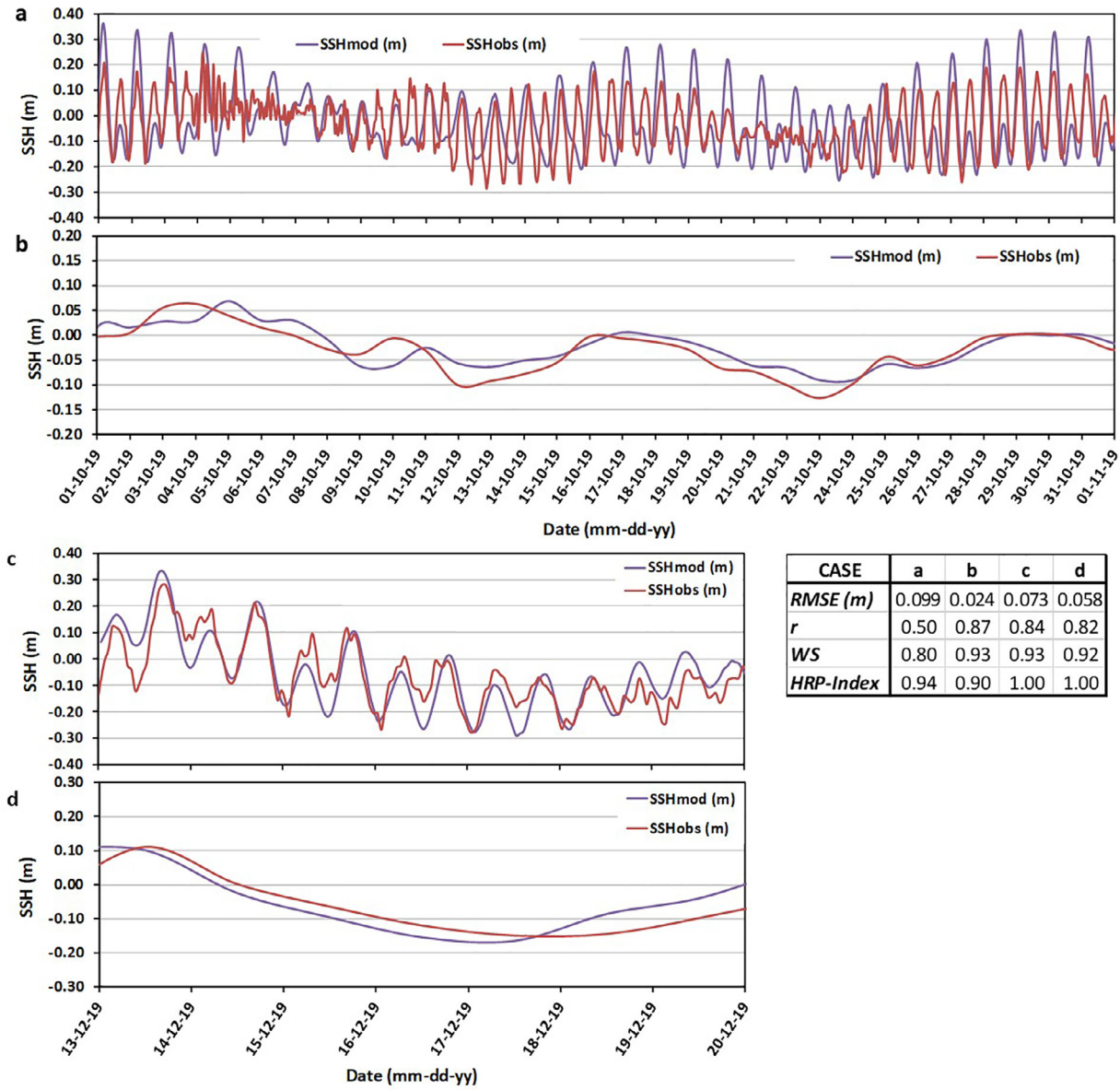

CASE	a	b	c	d
RMSE (m)	0.099	0.024	0.073	0.058
r	0.50	0.87	0.84	0.82
WS	0.80	0.93	0.93	0.92
HRP-Index	0.94	0.90	1.00	1.00

Fig. 11. Comparisons of model H operational forecast results (mod) against *in situ* observations (obs) of *SSH* (m) performed by our team during Autumn and Winter of 2019 in Thessaloniki port (see Fig. 3). Cases: a) hourly data and b) daily-averaged data for an entire month (October 2019); c) hourly data and d) daily-averaged data for an entire week (during December 2019). The following statistical measures are also provided in a table for quantitative validation; *WS*: Willmott Sill score; *RMSE*: root-mean-square error; *r*: Pearson correlation coefficient; *HRP*-index: Hit-Rate-of-Percentiles index.

Evaluation of model B's performance is also conducted by comparisons of simulation results with experimental data of multi-directional irregular wave diffraction around semi-infinite breakwaters and through breakwater gaps [42,89]. The incident significant wave height for the case of multi- and unidirectional irregular waves is $H_s = 0.055–0.0775$ and 0.0775 m, respectively; the peak spectral period is $T_p = 1.30$ s. Fig. 8 presents comparisons of model B results against experimental data in terms of diffraction coefficient K_D for quasi-irregular with relevant spreading parameter $s = 19$ or ∞ and two different initial angles of propagation. Results correspond to cross-sectional distributions of K_D at a distance $Y = 3L$ from the breakwaters. Comparisons of model results against experimental data are proven to be satisfactory, excelling especially for the case of unidirectional quasi-spectral wave propagation in the vicinity of port structures. Fig. 10 shows plausible representations, compared to relative experimental data, for the 2-D maps of calculated H/H_o for the case of a breakwater gap width $B = 3.92$ m ($B/L = 2$, L corresponding to peak period for quasi-irregular waves), under oblique (45°) and transverse (90°) wave attack. Instant depictions of η, after steady state is reached, are also given to represent the diffraction phenomenon and consequent ripple formation.

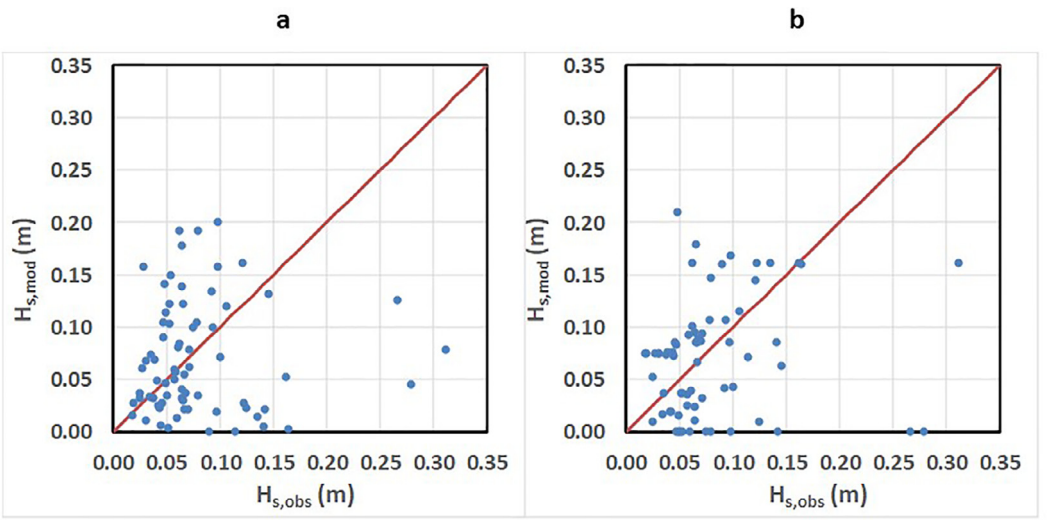

Thessaloniki
RMSE (m)
0.086
$RMSE/maxH_{s,obs}$
18.86%
r
0.317
WS
0.533
HRP-index
0.940

Fig. 12. Scatter plot comparisons of operational forecast results (mod) of significant wave height H_s (m) by a) model A and b) model B (forced on the boundary by model A output), against field data (obs) derived from the conducted *in situ* observations with the SBE26 wave gauge in Thessaloniki port (Fig. 3). Comparisons refer to a 3-day period of December 22nd – 24th 2019. The following statistical measures are also provided in a table for quantitative validation; *WS*: Willmott Sill score; *RMSE*: root-mean-square error; *r*: Pearson correlation coefficient; *HRP*-index: Hit-Rate-of-Percentiles index.

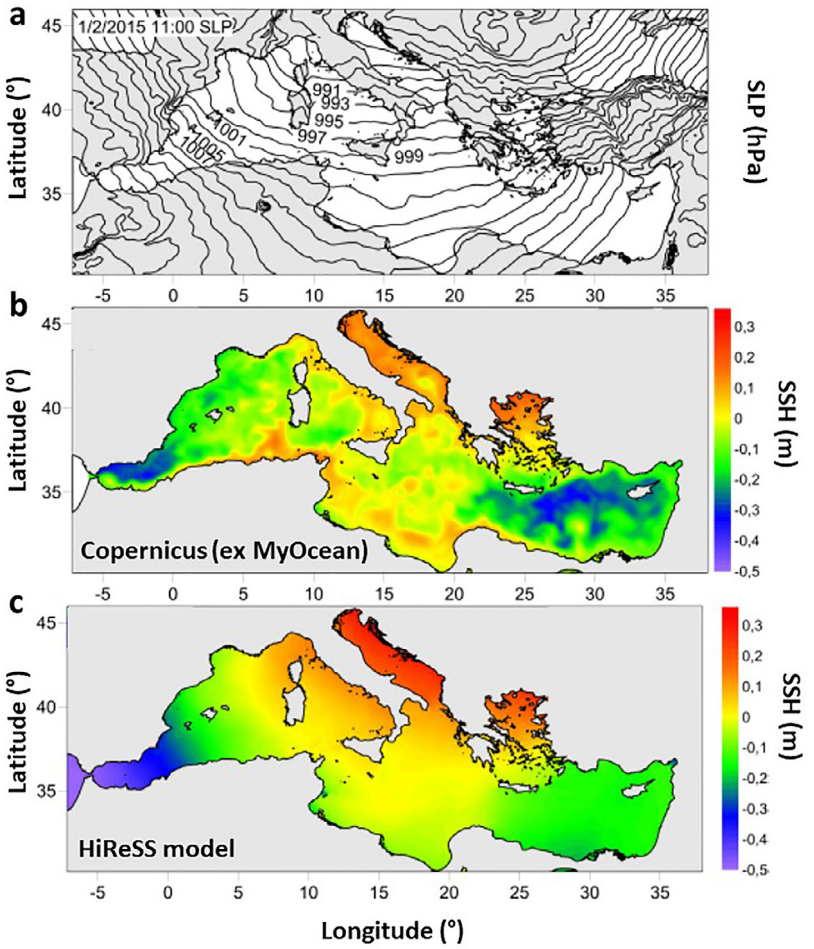

Fig. 13. Comparisons of operational forecasts for the spatial distribution of the free surface elevation due to storm surge SSH (m) in the Mediterranean Sea: a) Real weather barometric chart map created with data provided by [73]; b) Storm surge-induced sea level *SSH* (m) forecast by the Copernicus (*ex MyOcean*) platform [20]; c) Storm surge-induced sea level *SSH* (m) forecast with model H (HiReSS model used in [4] and [21]). Time of implementation: February 1st 2015, UTC 11:00.

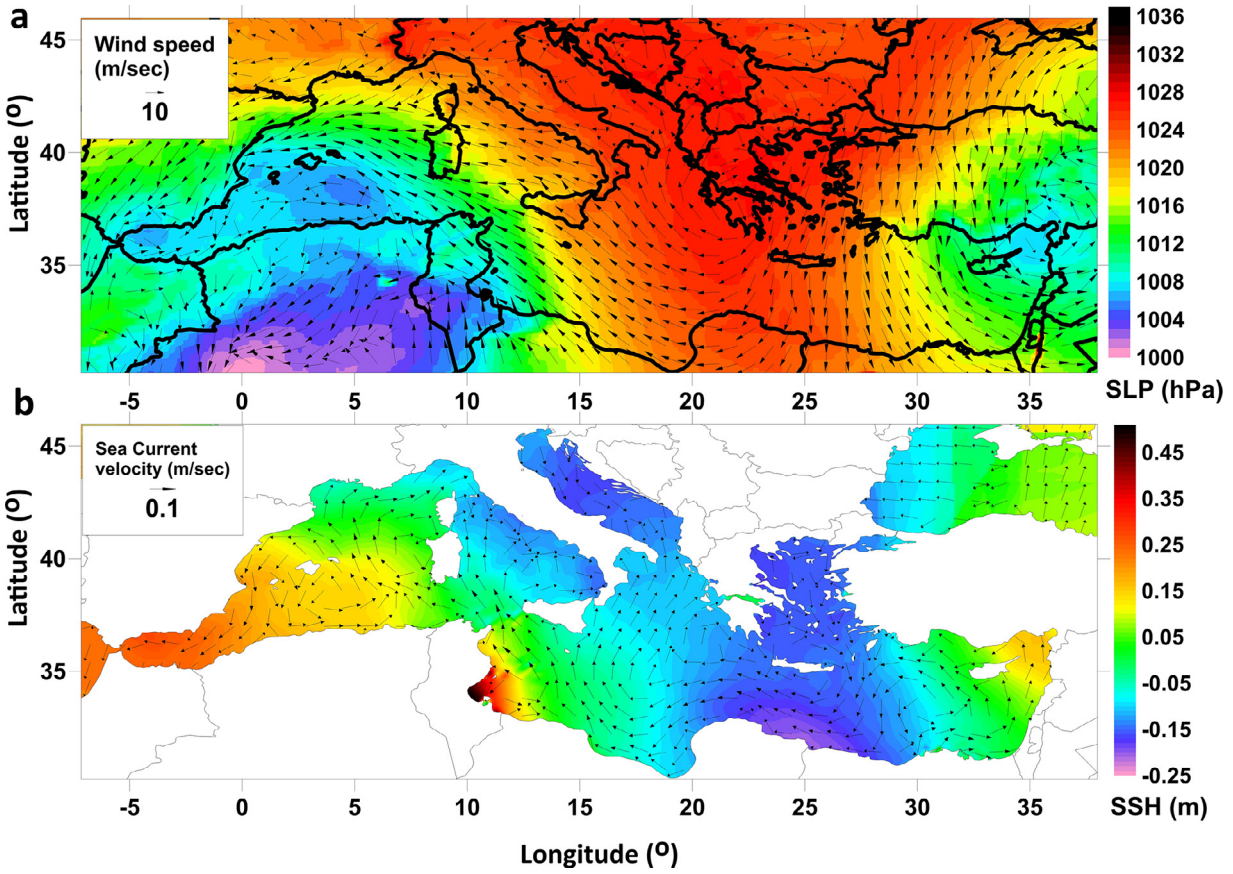

Fig. 14. a) Atmospheric weather conditions chart over southern Europe, where contours and color bar refer to *SLP* (hPa) and vectors to wind field speed (m/sec); b) Model H forecast results chart of the entire Mediterranean Sea basin, where contours and color bar refer to *SSH* (m) and vectors to sea current velocities (m/sec). Time of implementation: April 21st 2019, UTC 00:00.

3.4. Operational forecast validation

In order to evaluate all models' performance in operational mode, we performed further validation of HiReSS, TOMAWAC and WAVE-L forecast simulations against field data in Thessaloniki port (Fig. 2).

Fig. 11 presents comparisons of model H operational forecast results against *in situ* observations of *SSH* (m) performed by our team during autumn and winter of 2019 in Thessaloniki port (Section 3.1; Fig. 3). The investigated cases refer to both hourly (tide signal) and daily-averaged (surge signal) data mainly for an entire month (October 2019) and complementarily for a week during December 2019. Statistical measures were also computed for quantitative validation of model H runs (*WS, RMSE, r*, and *HRP*-index). Acceptable to very high correlation coefficient values and prediction skill were also achieved for the operational mode of model H, *e.g.* $r = 0.50–0.87$, $WS = 0.80–0.93$, *HRP*-index $= 0.9–1.0$ (Fig. 11). The errors in *SSH* present an upper limit of 7 cm being lower than 20% of the occurred *SSH* maxima. The latter are slightly over estimated by the model under certain weather conditions referring to the well-protected northern Thermaikos bay area. It can be deduced that the chosen spatial spacing of the computational domain provide efficient oceanographic predictions locally in coastal areas. We also note model H's ability to capture the local astronomical tide pattern in coastal areas, as the reproduced semi-diurnal tide signal is confirmed by reliable *in situ* data. The above are corroborated both in autumn and winter time periods. The weather-driven component of the surge-induced *SSH* forecasts can also be considered good, since modelled results remain close to *in situ* observations even on the daily-averaged signal (heuristically diminishing the tidal effects on the *SSH* signal).

Fig. 12 presents scatter plot comparisons of integrated model A and B operational forecast results for irregular and pseudo-spectral significant wave height H_s (m) against field data derived from the conducted *in situ* observations with the SBE26 wave gauge in Thessaloniki port (Fig. 3). Comparisons refer to a 3-day forecast period of December 22nd – 24t^{h} 2019. The calculated statistical measures are acceptable for the specific operational forecast case, particularly in very nearshore (rather shallow) waters, as they read: $WS = 0.533$, $RMSE = 8.6$ cm (corresponding to 18.86% of the maximum $H_{s,obs}$ for the 3-day forecast), $r = 0.317$, and *HRP*-index $= 0.94$. Based on the latter, the statistical distributions of percentiles for the modelled values are found to be close to the corresponding probabilistic properties of the observed H_s time series. For the evaluation of modelled spectral wave periods, we note that the irregular wave period that corresponds to H_s, i.e. T_s, reaches

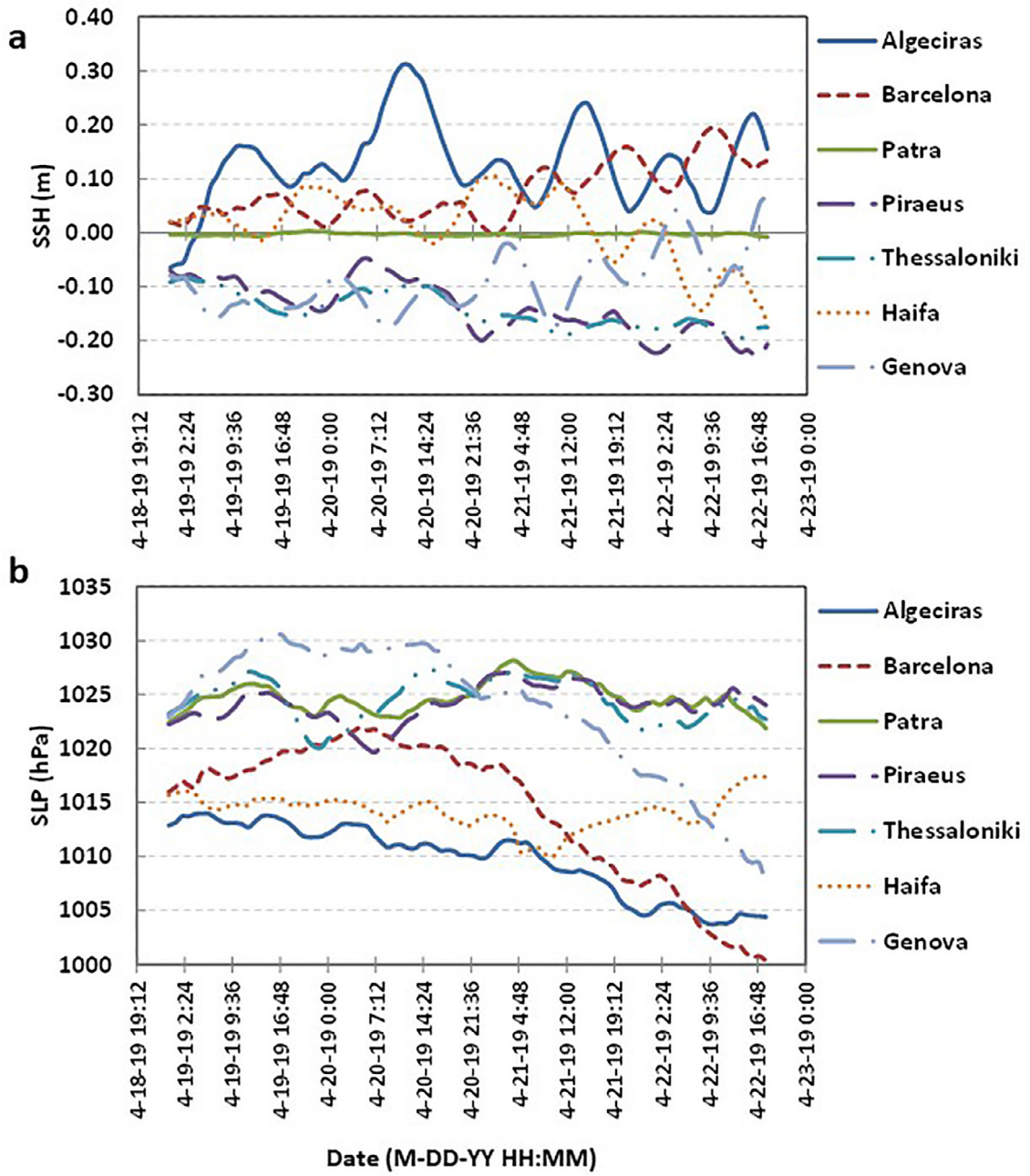

Fig. 15. Graphs of a) model H results about surge- and tide-induced *SSH* (m) and b) *SLP* (hPa) in seven characteristic ports of the Mediterranean basin (Algeciras, Barcelona, Genova, Haifa, Patra, Piraeus, Thessaloniki ports; Fig. 2). Forecasts refer to a 3-day period of April 19th - 22nd 2019.

an *RMSE* up to 0.81 sec, corresponding to only 13.83% of the maximum $T_{s,obs}$ for the 3-day forecast. Therefore, the integrated A and B models' implementation is found to have a plausible forecast performance skill, compared to operational wave predictions with 3rd generation spectral models by other researchers, *e.g.* [7–13]. Nevertheless, discrepancies between model results and field data still persist. The expected moderate performance of the used wave models in operational mode within coastal waters is highly influenced by two factors: a) the accuracy of input data [20] at the boundaries, and b) the fact that for small wave height and period (e.g. $H_s = 0.3$ m and $T_s = 3$ s), the deviations of model results relative to measurements are enhanced. This, however, will not practically affect the quality of our final product, since only larger waves (*e.g.* over 0.5 m) would be of interest for vessel pilotage. For these kinds of datasets, Copernicus [20] behaves well; preliminary comparisons of them against Poseidon [22] wave-buoy data in the central Aegean have confirmed this during the initial met-ocean input data evaluation phase (not shown for the sake of brevity).However, the integrated model A and B (*i.e.*

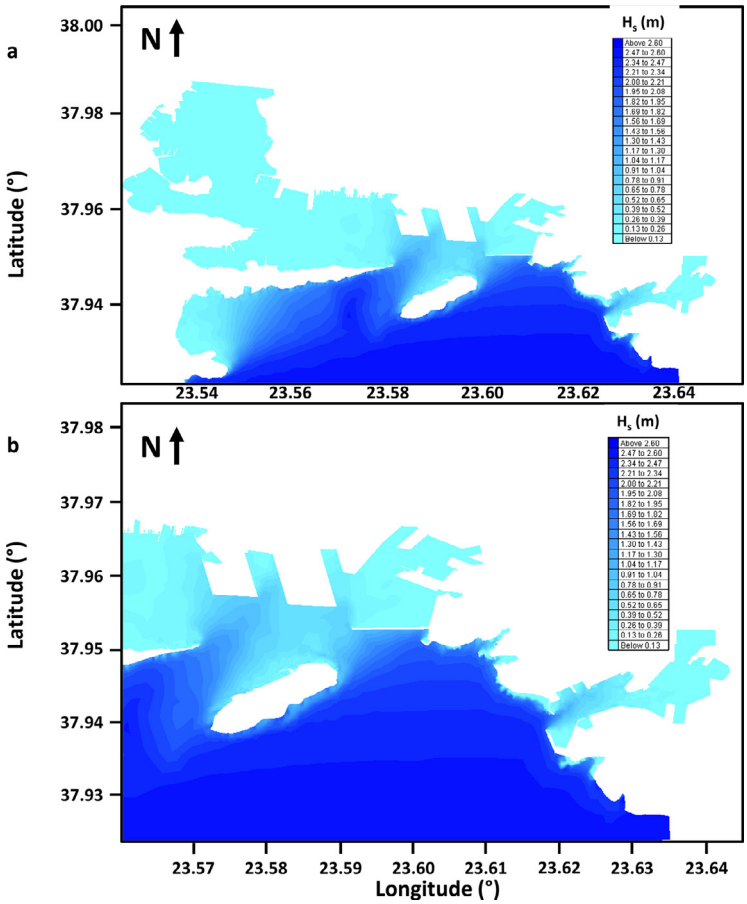

Fig. 16. Depiction of spatial distribution of significant wave height H_s (m) in operational forecast mode by simulation with model A inside and in the vicinity of the Piraeus port (Greece, west-central coast of the Aegean Sea; Fig. 2) for strong winds by the South sector (lower graph depicts a zoom-in version).

refined resolution model B, forced on the open boundary with numerical data by model A) simulations of nearshore wave characteristics seem to improve compared to the case of just applying the coarser model A near and inside ports. Hence, the integrated model A and B implementation in the vicinity of harbour structures within port areas seems capable of taking into account the fine and abrupt topographical changes in coastal areas and better reproduce phenomena as reflections from structures, diffraction and grouping of waves, etc.

The discrepancies between model results and field data are prominent, verifying the practical problems of operational forecast wave models in the existing literature to perform very well especially in nearshore areas. The major cause of the latter would probably be the coarse resolution of both meteorological forcing input and computational mesh, as well as the reliability of available global- or regional-scale boundary conditions in coastal areas. In addition, the refined resolution model B seems able to operationally reproduce mid- to shallow-water effects near and inside port basins.

4. Application of integrated models

Pilot implementations of the integrated sea-state forecast modelling system are presented in the Mediterranean Sea with a focus on several important ports in it (Fig. 2). In this Section we provide operational sea level and wave modelling output for characteristic Greek ports. The portrayed results concern maps and graphs of meteorologically and tidally induced *SSH*, depth-averaged hydrodynamic circulation and significant wave heights at steady state depictions of the 3-hourly time intervals for a 3-day forecast. This leads to the production of 24 representations of tide/surge and wave impacts for each daily implementation of the integrated forecast model.

4.1. Operational mode of model H

The operational function of model H in short-term, sea-level prediction mode has been also tested by a comparison with another available forecast product from the well-validated operational service of Copernicus platform [20], in the entire

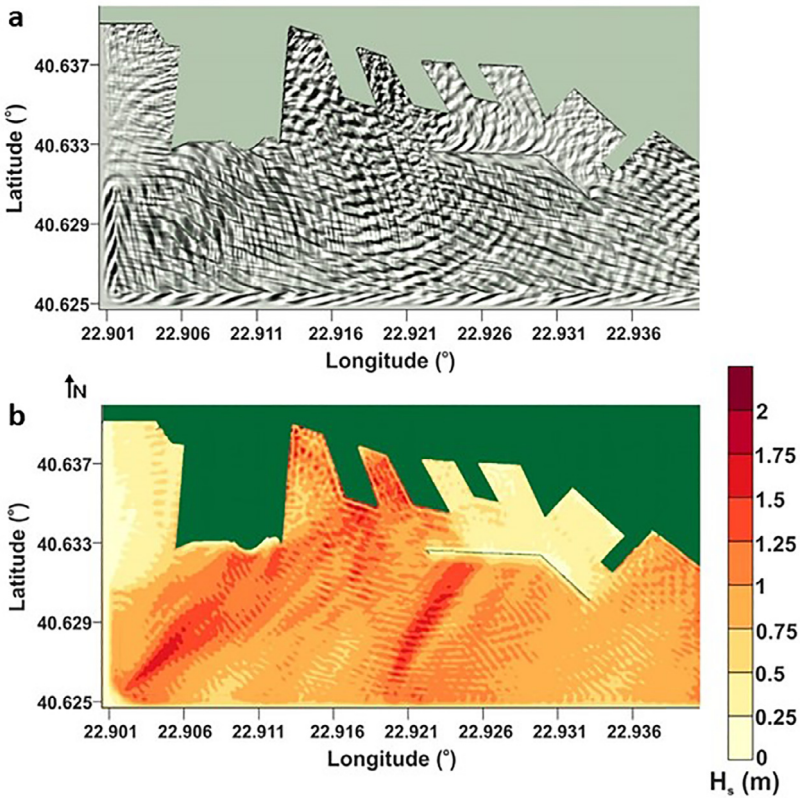

Fig. 17. Results charts in the Thessaloniki Port basin (Greece, northwestern coast of the Aegean Sea; Fig. 2) for a) wave-induced free surface elevation, and b) significant wave height H_s (m), in operational forecast mode by simulation with model B. Multi-directional, quasi-irregular high wave fields are shown approaching from the Southern-Southwestern sector referring to a steady-state representation of a selected 3-hourly sea state from a high seas period in May 2019; Peripheral sponge layer and eliminated reflections on lateral boundaries are also shown.

Mediterranean Sea. Fig. 13 presents model H operational forecasts of the sea surface elevation due to storm surge (*SSH*) in the Mediterranean basin, driven by a very low barometric system (cyclone with a minimum $SLP = 990$ hPa) over the Italian peninsula and the Adriatic Sea (Fig. 13c); the respective barometric chart is provided [73] is also presented in Fig. 13a. The HiReSS simulations are compared with Copernicus modelled fields (Fig. 13b). A comparable plausible depiction by the two modelling systems is obvious. The low barometric pressure ("bad" weather) influences the Adriatic and the North Aegean Seas producing $SSH > 30$ cm. The two modelling systems' results agree over the entire Mediterranean Sea [28,44].

It is also shown that the effects of the atmospheric pressure systems are strongly correlated to the SSH variability over the entire basin. Model H forecast results of simulated *SSH* fields and sea current speed in the entire Mediterranean Sea basin are presented in Fig. 14, in conjunction with atmospheric weather conditions (*SLP* and winds). Negative surges, *i.e.* sea surface below MSL, are apparent in the Adriatic and Aegean Seas, naturally due to the presence of a large barometric high ("good" weather) and northerly winds, driving waters southward away from the coast. On the contrary, large values of positive *SSH* are shown in the Gulf of Gabes and near the Gibraltar straits, which are influenced by the cyclonic motions of a low barometric system over the northwestern African coast, characterized by easterly winds. A secondary weaker low-pressure system over the eastern Mediterranean coast (~1008 hPa; Fig. 14a) also increased the sea level below the cyclone's core (inverse barometer effect) over the northeastern Levantine Sea (~15 cm; Fig. 14b). Westward and northward currents related to the atmospheric cyclonic wind circulation (Fig. 14a) were also well reproduced by model H over the western Mediterranean basin (2° *E* - 5° W; Fig. 14b) and the eastern Levantine basin (~35° *E*), respectively, contributing on the storm surge formation over these two areas. These examples confirm that model H may acceptably reproduce the effects of the inverse barometer effect in tandem with the wind-driven barotropic circulation on the sea level variations.

Fig. 15 presents characteristic *SSH* time series produced by model H forecasts in seven ports of the Mediterranean basin. Sea levels in Greek ports and Genova range from zero ("dead calm" sea state in Patra port) down to −20 cm, whereas storm-induced sea surface elevation is evident in Algeciras and Barcelona up to 30 cm. As expected, the *SLP* time series graph shows reversed patterns, corroborating the influence of the inverse barometer effect in these areas. Semi-diurnal undulating configurations are also clearly seen in the surge- and tide-driven *SSH* timeseries, revealing characteristic tidal elevation patterns in the Mediterranean Sea. Therefore, model H is found to successfully incorporate the tidal effects even if astronomic tidal ranges are considered to be insignificant in the specific region.

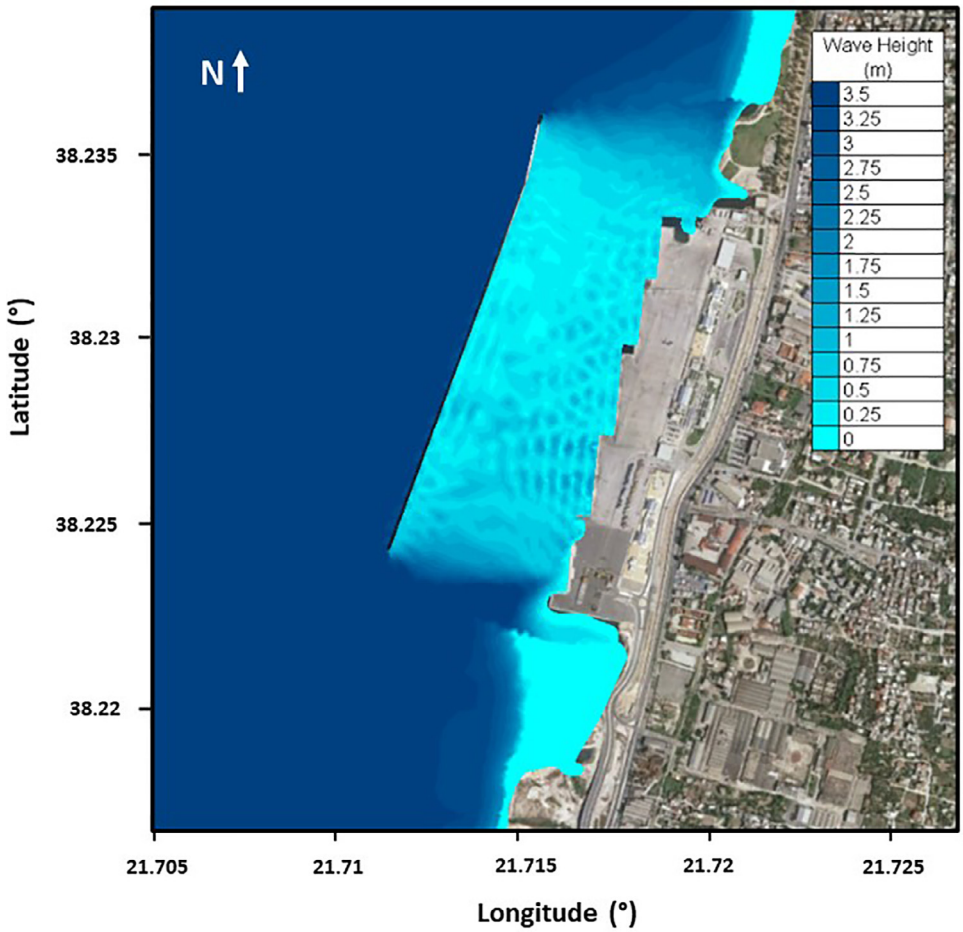

Fig. 18. Operational forecast results for spatial distribution of significant wave height H_s (m) by integrated simulation with models A and B inside and in the vicinity of the new Patra port (Greece, southeastern coast of the Ionian Sea; Fig. 2) for strong winds by the NW-W sector.

Conclusively, model H seems able to provide the necessary automated forecasts of sea levels (ranging at times from -0.80 m to +1 m) and currents in a characteristic large aquatic body (Mediterranean Sea) with refined information in diverse coastal areas near and inside ports.

4.2. Operational mode of wave models A and B

The results of pilot simulations with wave models A and B model mainly concern charts of mesh and gridded fields (or a combination of the two) producing maps of wave heights and propagation direction for spectral waves in coastal areas and quasi-regular waves inside ports. The presented maps comprise both models A and B domains, with the highest feasible spatial resolution (*i.e.* discretization step of $\Delta x = 2$ m) in port waters near the harbour structures, and $\Delta x = 25$–500 m in deeper waters, *e.g.* from narrow waterways and CNPs to offshore areas, respectively. Refinement of resolution is chosen in terms of the computational load, given the available resources and time for operational sea-state forecasting. Pilot results focus on the three largest commercial transit ports of Greece.

Fig. 16 depicts model A's forecasts of H_s inside and in the vicinity of the Piraeus port (Greece) for strong winds blowing from the southern sector. Wave penetration and agitation is minimal on the interior port facilities; H_s quickly reduces from 2.60 m in approach areas to values lower than 0.50 m in protected mooring canals and berthing locations. Sheltering effects leeward of insular formations and breakwaters, together with refraction of spectral waves in port waterways and canals, are simulated with acceptable accuracy by model A. However, for a detailed wave pattern portrayal by a phase-resolving model, Fig. 17 presents plotted results concerning simulated fields of gridded H_s data (as narrow-banded spectral wave fields) and relevant free-surface elevation, depicting steady-state conditions of an extreme case (incident $H_o = 2$ m) of southern seas in the Thessaloniki port basin. The protection offered by the sub-aerial breakwater is obvious, as transmitted H_s in the leeward side of the structure decreases by diffraction, reaching hardly up to 1/4 of the offshore wave height on the open boundary. Reflection patterns of the free surface elevation for multidirectional quasi-irregular waves are also visible in the

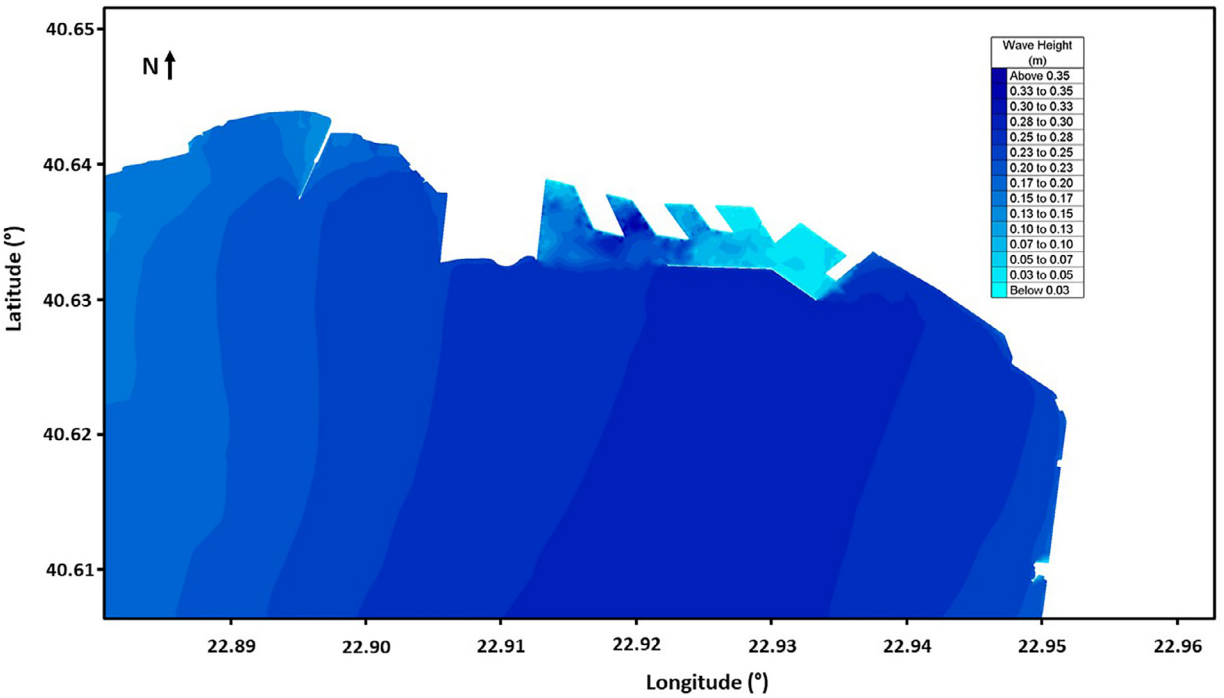

Fig. 19. Operational forecast results for the 2-DH spatial distribution of significant wave height H_s (m) by integrated simulation with models A and B in the Thessaloniki port (Greece, northwestern coast of the Aegean Sea; Fig. 2). Implementation refers to real-time operational forecasts for a 3-day period of December 22nd – 24th 2019; light winds by the SW-S sector.

port basin for the case of incident harsh sea states from the southern-southwestern sector. The resolution is very high in the case of model B and wave estimation accuracy is further ensured by the application of peripheral sponge layers and wave reflection techniques that eliminate unphysical reflections on lateral boundaries and structures; this discrepancy remains for phase-resolving wave models applied in harbour areas [97].

Fig. 18 presents the spatial distribution of an extreme case of H_s (>3.5 m) by integrated simulations with models A and B, inside and in the vicinity of an open-sea port, *i.e.* the new Patra port (southern Ionian Sea; Fig. 2), for strong winds blowing from the northwestern-northern sector. The synthesis of results from both wave models is achieved by a technique of densification of the mesh inside the port ensuring compatibility of the two model's mesh/grid. This way one can overall benefit from each model's distinct advantages and special features. Finally, Fig. 19 presents a typical steady-state condition of a 3-hour sea state corresponding to light winds by the SW-S sector in a physically protected port, *i.e.* Thessaloniki in the semi-enclosed Thermaikos Gulf at the northwestern coast of the Aegean Sea (Fig. 2). Results were produced by real-time, 3-day, operational forecasts during the period December 22nd – 24th 2019. The 2-DH spatial distribution of significant wave height H_s (m) is provided by integrated simulation with models A and B (fed by model H output for sea level). Consequently, the integrated model results are considered to form a novel complete body of information on sea states and weather conditions able to support pilotage guidance and, in general, safe approaching procedures of ship vessels to port and harbour basins.

5. Conclusions

In Accu-Waves project [4,5] a decision support tool is being developed to provide fine resolution forecasts on prevailing sea states at selected important ports of the Mediterranean basin (expanded to worldwide implementation in the future). The application will support approaching procedures of vessels to ports. In this paper, we present recent developments of a co-operating, high-resolution, hydrodynamic and wave model suite that derives data as boundary conditions from global-scale open-sea forecasts. Verification and application of hydrodynamic circulation, spectral and phase-resolving wave models for offshore, coastal areas and port basins were presented. Model coupling, nesting and integration are also attempted towards the materialization of a cloud-based operational forecast platform that will provide wind, wave, sea level and current data for a 3-day forecast at 3-hourly intervals in and around ports with global commercial interest and high transportation loads.

In the framework of an integrated tool for short-term marine weather and sea-state prognoses in broader areas around and inside harbours, a robust operational forecast model for storm surges was built. HiReSS (model H) was validated by comparisons of simulation output against sea level observations from tide gauges located in ports of the Mediterranean Sea.

It satisfactorily simulates the sea level variations inside harbour areas, also roughly estimating the mean sea currents there. Case studies in eight Mediterranean ports were presented. Results are also considered as crucial input (local bathymetric changes) in irregular wave simulations with the integrated TOMAWAC and WAVE-L models (A and B) sequence.

Furthermore, WAVE-L (model B) was validated by comparisons of model output against experimental data by classic laboratory physical simulations for both regular and spectral waves. It adequately simulates the wave propagation in nearshore areas over uneven bottoms and specifically the wave penetration inside harbours, around and on the leeward side of breakwaters, incorporating wave-structure interaction and plausible diffraction modelling. The presented case studies in characteristic Greek ports corroborate that. Conclusively, the integrated models are proved to satisfactorily simulate the sea surface elevation and wave characteristics in coastal areas over uneven beds and specifically inside pots, properly incorporating the wave-structure interaction.

Model H results address significant needs of port authorities, ship pilots and navigators towards battling problems of vessel impact on the harbour bed during mooring, towage and berth operations, according to high-resolution and short-term sea-state forecasting. The embedded A/B models' results address significant needs such as safe spatial and temporal planning of navigation towards and inside ports, port operations to and from mooring sites, while facilitating the ship-pilot and port-navigator consultation. This will allow more efficient management of the navigation and towage services. Indeed, the procedure to certify navigation paths in ports by ESA requires knowledge of operational conditions, including sea state and related environmental data. The safety issue is underlined also in the e-Navigation strategy by the IMO, where the aim is to analyze and provide quality marine weather data for limiting the environmentally driven human error in navigation.

Various tests of the combined hydrodynamic and wave models are ongoing and further pursued to check the robustness in specific port configurations and tackle a number of communication and performance problems among the models. Future research includes further site-specific validation of the operational phase of the models' performance, by conducting and utilizing further available *in situ* measurements in ports [20,72]. Moreover, certain methodologies should also be investigated in the future for possible port downtime identification and prediction, due to severe sea-state conditions, in-port seiching, and overtopping of harbour structures.

The new integrated modelling application seeks to address significant needs such as berth positions assignment according to auxiliary high-resolution, short-term weather and sea-state forecasts. This will significantly improve ports' arsenal towards reducing maritime accidents during these procedures, and thus assist on reduction of port downtime risk by delays in harbour serviceability and/or malfunction of port facilities, in the framework of digital support tools' update for Ports Safety Management Systems. All the above attest that the project's results constitute a very useful set of information that combine meteorological forecasts and hydrodynamic simulations of different scales with management data for port navigation and anchorage procedures.

Acknowledgements

This research has been co-financed by the European Union and Greek national funds through the Operational Program "Competitiveness, Entrepreneurship and Innovation", under the call "RESEARCH – CREATE – INNOVATE"; Project Name: ACCU-WAVES [4]; Project Code: T1EDK-05111. The authors are obliged to MarineTraffic [6] for providing Copernicus [20] and NOAA [72] input data, and to Assoc. Prof. Y. Pytharoulis from AUTh's Department of Meteorology and Climatology for providing regional weather predictions and local weather observations [73]. Initial configuration of HiReSS sea level forecasts was built within WaveForUs project [21], funded by the national action "COOPERATION 2011: Partnerships of Production and Research Institutions in Focused Research and Technology Sectors" in the framework of the operational program "Competitiveness and Entrepreneurship (NSRF2007-2013)". The tide-gauge data of sea level variations, used for HiReSS model validation, were provided by the HNHS [40].

References

[1] IMO, Report of the Maritime Safety Committee at its Eighty-Fifth Session, 2008.
[2] M. Porretta, D. Jimenez-Banos, M. Crisci, G. Solari, A. Fiumara, A. GNSS Evolution for Maritime an Incremental Approach, Inside GNSS, 2016.
[3] Marine Accident Investigation Branch, Department for Transport, UK, Safety Digest 2005-2009, Southampton
[4] Accu-Waves. A decision support tool for navigation management in ports. http://accuwaves.eu/ (accessed 12/10/2019)
[5] C. Memos, C. Makris, A. Metallinos, T. Karambas, D. Zissis, M. Chondros, G. Spiliopoulos, M. Emmanouilidou, A. Papadimitriou, V. Baltikas, Y. Kontos, G. Klonaris, Y. Androulidakis, V. Tsoukala, Accu-Waves: a decision support tool for navigation safety in ports, Proc. 1st DMPCO Conference, 2019.
[6] MarineTraffic, https://www.marinetraffic.com/ (accessed on 28/04/2020)
[7] W.E. Rogers, J.M. Kaihatu, L. Hsu, R.E. Jensen, J.D. Dykes, K.T. Holland, Forecasting and hindcasting waves with the SWAN model in the Southern California Bight, Coast. Eng. 54 (1) (2007) 1–15, doi:10.1016/j.coastaleng.2006.06.011.
[8] R. Allard, J. Dykes, Y.L. Hsu, J. Kaihatu, D. Conley, A real-time nearshore wave and current prediction system, J. Mar. Syst. 69 (1–2) (2008) 37–58.
[9] J.D. Dykes, D.W. Wang, J.W. Book, An evaluation of a high-resolution operational wave forecasting system in the Adriatic Sea, J. Mar. Syst. 78 (2009) S255–S271.
[10] G. Singhal, V.G. Panchang, J.L. Lillibridge, Reliability assessment for operational wave forecasting system in Prince William Sound, Alaska, J. Waterway Port Coast. Ocean Eng. 136 (6) (2010) 337–349.
[11] J.R. Bidlot, Present status of wave forecasting at ECMWF, in: Proceeding from the ECMWF workshop on ocean waves, 2012, June, pp. 25–27.
[12] A. Chawla, H.L. Tolman, V. Gerald, D. Spindler, T. Spindler, J.H.G. Alves, D. Cao, J.L. Hanson, E.M. Devaliere, A multigrid wave forecasting model: a new paradigm in operational wave forecasting, Weather Forecast. 28 (4) (2013) 1057–1078.
[13] L. Rusu, C.G. Soares, Evaluation of a high-resolution wave forecasting system for the approaches to ports, Ocean Eng. 58 (2013) 224–238.
[14] M. Baldauf, S.B. Hong, Improving and Assessing the impact of e-Navigation applications, Int. J. e-Navig. Mar. Econ. 4 (2016) 1–12.

[15] A. Weintrit, T. Neumann, Marine navigation and safety of sea transportation: STCW, Maritime Education and Training (MET), human resources and crew manning, maritime policy, Logistics and Economic Matters, CRC Press, 2013.
[16] IMO, e-Navigation Strategy Implementation Plan, 2014.
[17] Improved Port Efficiency And Safety Using A Novel Wireless Network And Differential Global Navigation Satellite System Providing Enhanced Vessel Navigation, http://www.dockingassist.eu/ (accessed 23/04/2020)
[18] PORTS® Physical Oceanographic Real-Time System, https://tidesandcurrents.noaa.gov/ports.html, (accessed 23/04/2020)
[19] New AVANTI port information software, https://safety4sea.com/new-avanti-port-information-software/ (accessed 23/04/2020)
[20] COPERNICUS MARINE ENVIRONMENT MONITORING SERVICE, Providing PRODUCTS and SERVICES for all marine applications, http://marine.copernicus.eu/ (accessed 12/10/2019)
[21] WaveForUs: A pilot system for the development and delivery of daily wave and circulation forecasts for public and emergency use in the Thermaikos gulf, http://wave4us.web.auth.gr/ (accessed 23/04/2020)
[22] Poseidon System: Monitoring, Forecasting and Information System for the Greek Seas, http://www.poseidon.hcmr.gr/ (accessed 23/04/2020)
[23] KASSANDRA Storm Surge Modelling System, http://kassandra.ve.ismar.cnr.it:8080/kassandra (accessed 23/04/2020)
[24] SOCIB – WMOP, http://thredds.socib.es/ (accessed 23/04/2020)
[25] COSYNA - Coastal Observing System for Northern and Arctic Seas, https://www.hzg.de/institutes_platforms/cosyna/index.php.en (accessed 23/04/2020)
[26] Y.S. Androulidakis, K.D. Kombiadou, C.V. Makris, V.N. Baltikas, Y.N. Krestenitis, Storm surges in the Mediterranean Sea: Variability and trends under future climatic conditions, Dyn. Atmos. Ocean. (2015), doi:10.1016/j.dynatmoce.2015.06.001.
[27] Y.N. Krestenitis, Y.S. Androulidakis, Y.N. Kontos, G. Georgakopoulos, Coastal inundation in the north-eastern mediterranean coastal zone due to storm surge events, J. Coast. Conserv. 15 (2011) 353–368, doi:10.1007/s11852-010-0090-7.
[28] Y. Krestenitis, I. Pytharoulis, T.S. Karacostas, Y. Androulidakis, C. Makris, K. Kombiadou, I. Tegoulias, V. Baltikas, S. Kotsopoulos, S. Kartsios, Severe weather events and sea level variability over the mediterranean sea: the waveforus operational platform, in: 2017. doi:10.1007/978-3-319-35095-0_9.
[29] C.V. Makris, Y.S. Androulidakis, Y.N. Krestenitis, K. Kombiadou, V.N. Baltikas, Numerical modelling of storm surges in the Mediterranean sea under climate change, 36th IAHR World Congr., 2015.
[30] C. Makris, P. Galiatsatou, K. Tolika, C. Anagnostopoulou, K. Kombiadou, P. Prinos, K. Velikou, Z. Kapelonis, E. Tragou, Y. Androulidakis, G. Athanassoulis, C. Vagenas, I. Tegoulias, V. Baltikas, Y. Krestenitis, T. Gerostathis, K. Belibassakis, E. Rusu, Climate change effects on the marine characteristics of the Aegean and Ionian Seas, Ocean Dyn. (2016), doi:10.1007/s10236-016-1008-1.
[31] C. Makris, Y. Androulidakis, V. Baltikas, Y. Kontos, T. Karambas, Y. Krestenitis, HiReSS: Storm surge simulation model for the operational forecasting of sea level elevation and currents in marine areas with harbor works, in: Proc. 1st DMPCO Conference, 2019.
[32] Open TELEMAC-MASCARET. The mathematically superior suite of solvers. TOMAWAC - Wave propagation in coastal areas, http://www.opentelemac.org/index.php/presentation?id=20 (accessed 12/10/2019)
[33] M. Benoit, F. Marcos, F. Becq, Development of a third generation shallow-water wave model with unstructured spatial meshing, Proc. Coast. Eng. Conf. (1996).
[34] M. Benoit, F. Marcos, F. Becq, TOMAWAC: a prediction model for offshore and nearshore storm waves, in: Proceedings, Congr. Int. Assoc. Hydraul. Res. IAHR, 1997.
[35] J.M. Hervouet, TELEMAC, a Hydroinformatic System, Houille Blanche, 1999, doi:10.1051/lhb/1999029.
[36] R. Issa, D. Rougé, M. Benoit, D. Violeau, A. Joly, Modelling algae transport in coastal areas with a shallow water equation model including wave effects, J. Hydro-Environ. Res. (2010), doi:10.1016/j.jher.2009.10.004.
[37] T.V. Karambas, S. Christopoulos, I. Avgeris, HARBOUR_L: integrated mathematical model for the design of harbor works, 5th Pan-Hellenic Conf. Harb. Work., 2010.
[38] T.V. Karambas, A.G. Samaras, An integrated numerical model for the design of coastal protection structures, J. Mar. Sci. Eng. (2017), doi:10.3390/jmse5040050.
[39] C. Makris, T. Karambas, V. Baltikas, Y. Kontos, A. Metallinos, M. Chondros, A. Papadimitriou, V. Tsoukala, C. Memos, WAVE-L: an integrated numerical model for wave propagation forecasting in harbor areas, in: Proc. 1st DMPCO Conference, 2019.
[40] Hellenic Navy Hydrographic Service (HNHS), https://www.hnhs.gr/en/ (accessed 12/10/2019)
[41] C.L. Vincent, M.J. Briggs, Refraction—diffraction of irregular waves over a mound, J. Waterw Port Coast. Ocean Eng. (1989), doi:10.1061/(ASCE)0733-950X(1989)115:2(269).
[42] Y.X. Yu, S.X. Liu, Y.S. Li, O.W.H. Wai, Refraction and diffraction of random waves through breakwater, Ocean Eng. (2000), doi:10.1016/S0029-8018(99)00005-0.
[43] H. de Vries, M. Breton, T. de Mulder, Y. Krestenitis, J. Ozer, R. Proctor, K. Ruddick, J.C. Salomon, A. Voorrips, A comparison of 2D storm surge models applied to three shallow European seas, Environ. Softw. (1995), doi:10.1016/0266-9838(95)00003-4.
[44] Y.N. Krestenitis, Y. Androulidakis, K. Kombiadou, C. Makris, V. Baltikas, G. Kalantzi, Operational oceanographic forecasts in the Thermaikos gulf: the waveforus project, in: Proc. 12th Int. Conf. Prot. Restor. Environ., 2014.
[45] Υ. Krestenitis, K. Kombiadou, Y.S. Androulidakis, C. Makris, V. Baltikas, C. Skoulikaris, Y.N. Kontos, G. Kalantzi, Operational oceanographic platform in Thermaikos Gulf (Greece): forecasting and emergency alert system for public use, in: Proc. 36th IAHR World Congress, 2015.
[46] Y Krestenitis, Y Androulidakis, K Kombiadou, C Makris, V Baltikas, Operational forecast system of storm tides in the Aegean Sea (Greece), in: Proc. 2015 ASLO Aquat. Sci. Meet., 2015.
[47] X.H. Wang, Tide-induced sediment resuspension and the bottom boundary layer in an idealized estuary with a muddy bed, J. Phys. Oceanogr. (2002), doi:10.1175/1520-0485(2002)032⟨3113:TISRAT⟩2.0.CO;2.
[48] S.D. Smith, E.G. Banke, Variation of the sea surface drag coefficient with wind speed, Q. J. R. Meteorol. Soc. (1975), doi:10.1002/qj.49710142920.
[49] P.J. Roache, Computational Fluid Dynamics, Hermosa, Albuquerque, 1972.
[50] E.W. Schwiderski, On charting global ocean tides, Rev. Geophys. (1980), doi:10.1029/RG018i001p00243.
[51] K. Sakamoto, H. Tsujino, H. Nakano, M. Hirabara, G. Yamanaka, A practical scheme to introduce explicit tidal forcing into an OGCM, Ocean Sci. (2013), doi:10.5194/os-9-1089-2013.
[52] K. Matsumoto, T. Takanezawa, M. Ooe, Ocean tide models developed by assimilating TOPEX/POSEIDON altimeter data into hydrodynamical model: A global model and a regional model around Japan, J. Oceanogr. (2000), doi:10.1023/A:1011157212596.
[53] P. Schureman, Manual of harmonic analysis and prediction of tides, 1958. doi:10.5962/bhl.title.38116.
[54] C.C. Mei, The applied dynamics of ocean surface waves., (1983).
[55] H.L. Tolman, A third-generation model for wind waves on slowly varying, unsteady, and inhomogeneous depths and currents, J. Phys. Oceanogr. (1991), doi:10.1175/1520-0485(1991)021⟨0782:atgmfw⟩2.0.co;2.
[56] G.J. Komen, L. Cavaleri, M. Donelan, K. Hasselmann, S. Hasselmann, P.A.E.M. Janssen, Dynamics and Modelling of Ocean Waves, Cambridge University Press, Cambridge, 1994, doi:10.1017/CBO9780511628955.
[57] TOMAWAC User Manual, http://wiki.opentelemac.org/doku.php?id=user_manual_tomawac (accessed 12/10/2019)
[58] K. Hasselmann, S. Hasselmann, E. Bauer, P.A.E.M. Janssen, G.J. Komen, L. Bertotti, P. Lionello, A. Guillaume, V.C. Cardone, J.A. Greenwood, M. Reistad, L. Zambresky, J.A. Ewing, The WAM model - a third generation ocean wave prediction model., J. Phys. Ocean (1988).
[59] G.J.M. Copeland, A practical alternative to the “mild-slope” wave equation, Coast. Eng. (1985), doi:10.1016/0378-3839(85)90002-X.
[60] A. Watanabe, K. Maruyama, Numerical modeling of nearshore wave field under combined refraction, diffraction and breaking, Coast. Eng. Jpn. 29 (1986) 19–39, doi:10.1080/05785634.1986.11924425.
[61] S. Christopoulos, I. Avgeris, T.V. Karambas, HMAR-HARBOURL: an integrated numerical model for harbour layout design, in: Proc. Int. Soc. Offshore Polar Eng. Conf., ISOPE, 2012.

[62] J.A. Battjes, J.P.F.M. Janssen, Energy loss and set-up due to breaking of random waves, in: Proc. Coast. Eng. Conf., 1, 1979, pp. 569–587.
[63] W. Rattanapitikon, R. Karunchintadit, T. Shibayama, Irregular wave height transformation using representative wave approach, Coast. Eng. J. (2003), doi:10.1142/S0578563403000865.
[64] J. Larsen, H. Dancy, Open boundaries in short wave simulations – a new approach, Regelungstechnik RT (1983), doi:10.1016/0378-3839(83)90022-4.
[65] C. Lee, K.D. Suh, Internal generation of waves for time-dependent mild-slope equations, Coast. Eng. (1998), doi:10.1016/S0378-3839(98)00012-X.
[66] T.V. Karambas, B.C. Bowers, Representation of partial wave reflection and transmission for rubble mound coastal structures, WIT Trans. Ecol. Environ. (1996) 18, doi:10.2495/HY960421.
[67] P. Bruun, Design and Construction of Mounds for Breakwaters and Coastal Protection, Elsevier, Amsterdam, The Netherland, 1985.
[68] C.G. Koutitas, Numerical solution of the complete equations for nearly horizontal flows, Adv. Water Resour. 1 (1978) 213–217, doi:10.1016/0309-1708(78)90005-2.
[69] T.V. Karambas, C.D. Memos, Boussinesq model for weakly nonlinear fully dispersive water waves, J. Waterw. Port Coast. Ocean Eng. (2009), doi:10.1061/(ASCE)0733-950X(2009)135:5(187).
[70] MEDITERRANEAN SEA PHYSICS ANALYSIS AND FORECAST, Metadata Provided by CMEMS, E.U. Copernicus Marine Service Information, https://doi.org/10.25423/CMCC/MEDSEA_ANALYSIS_FORECAST_PHY_006_013_EAS5 (accessed on 28/04/2020)
[71] E. Clementi, J. Pistoia, R. Escudier, D. Delrosso, M. Drudi, A. Grandi, R. Lecci, S. Cretí, S. Ciliberti, G. Coppini, S. Masina, N. Pinardi, Mediterranean Sea Analysis and Forecast (CMEMS MED-Currents, EAS5 system) [Data set], Copernicus Monitoring Environment Marine Service (CMEMS), 2019.
[72] National Oceanic and Atmospheric Administration, National Centers for Environmental Information, Model Data, Global Forecast System (GFS), https://www.ncdc.noaa.gov/data-access/model-data/model-datasets/global-forcast-system-gfs (accessed 12/10/2019)
[73] AUTh, Department of meteorology and climatology, meteorological observations online service, https://meteo.geo.auth.gr/en/meteo-obs (accessed 23/04/2020)
[74] I. Tegoulias, S. Kartsios, I. Pytharoulis, S. Kotsopoulos, T.S. Karacostas, The influence of WRF parameterisation schemes on high resolution simulations over Greece, in: In Perspectives on Atmospheric Sciences, Springer, 2017, pp. 3–8.
[75] I. Pytharoulis, I. Tegoulias, S. Kotsopoulos, D. Bampzelis, S. Kartsios, P. Zanis, et al., High-resolution WRF hindcasts over central Greece: Characteristics of simulated convective activity and model evaluation, in: Proc.: 15th Annual WRF Users' Workshop, Boulder, CO, 2014, pp. 23–27.
[76] I. Pytharoulis, T. Karacostas, I. Tegoulias, S. Kotsopoulos, D. Bampzelis, Predictability of intense weather events over Northern Greece, in: Proc.: 95th American Meteorological Society Annual Meeting, Phoenix, AZ, USA, 2015, p. 895.
[77] MEDITERRANEAN SEA WAVES ANALYSIS AND FORECAST, Metadata provided by CMEMS, E.U. Copernicus Marine Service Information, https://doi.org/10.25423/CMCC/MEDSEA_ANALYSIS_FORECAST_WAV_006_017 (accessed on 28/04/2020)
[78] G. Korres, M. Ravdas, A. Zacharioudaki, Mediterranean Sea Waves Analysis and Forecast (CMEMS MED-Waves) [Data set], Copernicus Monitoring Environment Marine Service (CMEMS), 2019 https://doi.org/10.25423/CMCC/MEDSEA_ANALYSIS_FORECAST_WAV_006_017.
[79] Navionics, https://webapp.navionics.com/ (accessed 12/10/2019)
[80] General Bathymetric Chart of the Oceans (GEBCO), www.gebco.net (accessed 12/10/2019)
[81] Y. Goda, Y. Suzuki, Computation of Refraction and Diffraction of Sea Waves With Mitsuyasu's Directional Spectrum, 1975.
[82] Sea-Bird Scientific, CTDs, Moored, SBE 26plus Seagauge Wave & Tide Recorder https://www.seabird.com/moored/sbe-26plus-seagauge-wave-tide-recorder-discontinued/family?productCategoryId=54627473779 (accessed 23/04/2020)
[83] Sea-Bird Scientific, Software, https://www.seabird.com/software (accessed 23/04/2020)
[84] Sea-bird Scientific, SBE 26plus Seagauge Wave & Tide Recorder, User Manual, 2015.
[85] Global Sea Level Observing System (GLOSS), https://www.gloss-sealevel.org/fast-mode-data-delivery (accessed 12/10/2019)
[86] Italian National Institute for Environmental Protection and Research (ISPRA) http://www.isprambiente.gov.it/pre_mare/coastal_system/maps/mc_wiz.html (accessed 12/10/2019)
[87] D. Conte, P. Lionello, Characteristics of large positive and negative surges in the Mediterranean Sea and their attenuation in future climate scenarios, Glob. Planet. Change (2013), doi:10.1016/j.gloplacha.2013.09.006.
[88] R. Pawlowicz, B. Beardsley, S. Lentz, Classical tidal harmonic analysis including error estimates in MATLAB using T TIDE, Comput. Geosci. (2002), doi:10.1016/S0098-3004(02)00013-4.
[89] Y.S. Li, S.X. Liu, Y.X. Yu, G.Z. Lai, Numerical modelling of multi-directional irregular waves through breakwaters, Appl. Math. Model. (2000), doi:10.1016/S0307-904X(00)00003-2.
[90] C.J. Willmott, S.M. Robeson, K. Matsuura, A refined index of model performance, Int. J. Climatol. (2012), doi:10.1002/joc.2419.
[91] P. Galiatsatou, C. Makris, P. Prinos, D. Kokkinos, Nonstationary joint probability analysis of extreme marine variables to assess design water levels at the shoreline in a changing climate, Nat. Hazard. (2019), doi:10.1007/s11069-019-03645-w.
[92] Y. Galiatsatou, C. Makris, D. Kokkinos, P. Prinos, Y. Krestenitis, Climate change effects on extreme total water levels of the Greek coastal zone, in: Proc. 1st DMPCO Conference, DMPCO, 2019.
[93] C. Makris, P. Galiatsatou, Y. Androulidakis, K. Kombiadou, V. Baltikas, Y. Krestenitis, P. Prinos, Climate change impacts on the coastal sea level extremes of the east-central Mediterranean Sea, XIV PRE Conference, 2018.
[94] R. Schoetter, P. Hoffmann, D. Rechid, K.H. Schlünzen, Evaluation and bias correction of regional climate model results using model evaluation measures, J. Appl. Meteorol. Climatol. (2012), doi:10.1175/JAMC-D-11-0161.1.
[95] T. Awk, TOMAWAC v7p3 Validation Manual, 2018.
[96] J.C.W. Berkhoff, N. Booy, A.C. Radder, Verification of numerical wave propagation models for simple harmonic linear water waves, Coast. Eng. (1982), doi:10.1016/0378-3839(82)90022-9.
[97] T. Karambas, C. Makris, V. Baltikas, 2-DH Post-Boussinesq modeling of nonlinear wave propagation and transformation in Nearshore zones and inside ports, Proc. Coast. Struct. Conf. (2019).